DYNAMIC COMPLEX SMART COLLOIDS FOR THE DETECTION OF BIOMOLECULES

by

Qifan Zhang

B.S., Chemistry

University of Illinois at Urbana-Champaign, 2013

Submitted to the Department of Chemistry in Partial Fulfillment of the

Requirements for the Degree of

Doctor of Philosophy in Inorganic Chemistry

at the

MASSACHUSETTS INSTITUTE OF TECHNOLOGY

June 2018

Signature redacted

Signature of Author: ....

Department of Chemistry

Signature redacted

May 10, 2018

Certified by: ....

Timothy M. Swager

John D. MacArthur Professor of Chemistry

Signature redacted Thesis Supervisor

Accepted by: ....

Robert W. Field

Haslam and Dewey Professor of Chemistry

Chairman, Departmental Committee on Graduate Students

This doctoral thesis has been examined by a

Committee of the Department of Chemistry as follows:

Signature redacted

Professor Christopher C. Cummins..... .....

Department of Chemistry

Thesis Committee Chairman

Signature redacted

Professor Timothy M. Swager..... .....

Department of Chemistry

Thesis Advisor

Signature redacted

Professor Yogesh Surendranath.....

Department of Chemistry

Committee Member

DYNAMIC COMPLEX SMART COLLOIDS FOR THE DETECTION OF BIOMOLECULES

by

Qifan Zhang

Submitted to the Department of Chemistry in Partial Fulfillment of the Requirements for the Degree of Doctor of Philosophy in Chemistry

ABSTRACT

Complex smart colloid is a new class of dynamically reconfigurable emulsion droplets that switch morphologies between encapsulated and Janus configuration upon binding to chemical and biological analytes. The changes of morphologies or orientations of the Janus droplets are readily detected with an optical transduction mechanism. The dynamic complex smart colloids are ideal sensing particles for aqueous sensing of biomolecules such as bacteria, oligonucleotide, antibodies and viruses.

This thesis expands the applications of complex smart colloids as bioassays that can be potentially adopted in food and beverage industry, environmental monitoring and medical diagnostics. In Chapter 2, we demonstrate an example of using emulsion agglutination assay for E.*coli* sensing with a continuous phase carbohydrate surfactant. In Chapter 3, we expand the emulsion assay by using interfacial bioconjugation methods and eliminating the needs of a synthetic surfactant in the continuous phase. In Chapter 4, we develop the protein-protein agglutination assay with a thermal stable protein conjugate to the droplet-water interface for sensing of Zika protein NS1.

Thesis Supervisor: Timothy M. Swager

Title: John D. MacArthur Professor of Chemistry

Table of Contents

List of Figures

List of Schemes

Chapter 1

Introduction

1.1 Sensors

Low cost, low power, and portable chemical/biological sensors can be practical alternatives to conventional analytical instrumentation for various applications,[1] such as food testing, environmental monitoring, and homeland security. Sensors respond to local environmental change with an analytically useful signal. The design of innovative sensing materials, including carbon nanotubes, graphenes, polymers and even functionalized papers, provides new opportunities to transform the core chemical/biological recognition into a digitalized signal. These types of sensors have huge cost and accessibility advantage over conventional analytical instrumentation, which requires large capital upfront investment and proficient technicians.

The sensing materials have to be carefully selected for the suitable applications. Carbon based nano-materials for example are ideal for gas sensing because of their high surface areas for gas molecule recognition and changes in electronic resistance for signals.[2] Aqueous sensing on the other hand can be challenging when there is high electrolyte conductance background in the continuous phase, which is common for most of the bioassays.

1.2 Colloid and Liquid Emulsion Sensors

Colloidal nano-and micro-particle based materials have attracted a great deal of attention in the past decades, particularly in biological sciences and diagnostics.[3] The colloidal system is a multiphasic platform that combines different functionalities into a single carrier system. Additionally, the simple fabrication process, long stability, design flexibility provides promises to mimic live cells in biological systems. Colloidal sensors range from single and micro nanoparticles (NPs)[4] to complex hybrid microstructures[5] and have been widely used for sensing of biomolecules including nucleotides,[6] antibodies,[7] bacteria[8] and viruses.[9]

Liquid emulsions, are a class of colloidal materials, wherein a mixture of two or more immiscible liquids are stabilized by surfactants to give particles. Liquid components are dispersed in a continuous liquid phase forming simple or complex emulsions. Complex emulsions with different geometries and compositions, including Janus emulsions (droplets with faces that exhibit differing physical properties) and multiple emulsions have recently become a focus of research interest because of their promising applications in pharmaceuticals[10], medical diagnostics[11], cosmetics[12], dynamic optics[13] and chemical separations[14]. Emulsions are mostly fabricated using microfluidics,[15] ultrasonic or membrane extrusion.[16] Emulsion droplets can also function as cargos carrying active drug molecules and have been studied extensively in the field of drug delivery.[17]

Most of the liquid emulsion reported as sensors in the literature are around liquid crystal (LCs) emulsion droplets.[18] The high sensitivity of the LC emulsion droplets attributes to their intrinsic optical properties and the change of orientational order associated with the molecular-level recognition at the LC interface.[19] A more ideal emulsion based sensor system would be able to maintain these optical properties but also provides more capabilities of functionalization at the interface for specific binding of the chemical and biological analytes.

1.3 Dynamic Smart Colloids as Sensors

Our group recently reported a new class of dynamically reconfigurable complex emulsion droplets that can switch their morphology between encapsulated and Janus configurations upon exposure to external stimuli.[20] The change of morphologies between hydrocarbon-in-fluorocarbon-in-water (H/F/W), Janus and fluorocarbon-in-hydrocarbon-in-water (F/H/W) induced by varying of the interfacial tensions could serve as a transduction mechanism for sensing of the chemical and biological analytes.

This type of complex emulsion is composed of a hydrocarbon phase and a fluorocarbon phase surrounded by a continuous water phase with surfactants. Based on the fact that the selected fluorocarbons (FCs) and hydrocarbons (HCs) are immiscible at room temperature but miscible with gentle heating (low upper critical temperature, T_c), we first disperse a single phase of a FC and HC mixture at elevated temperature and then cool them down to generate double emulsions (**Fig. 1.1a**). The polydisperse droplets can be easily manufactured in bulk via simple emulsification process with the exact same composition. The complex emulsion droplets thus provide the bases of a type of low cost sensor material.

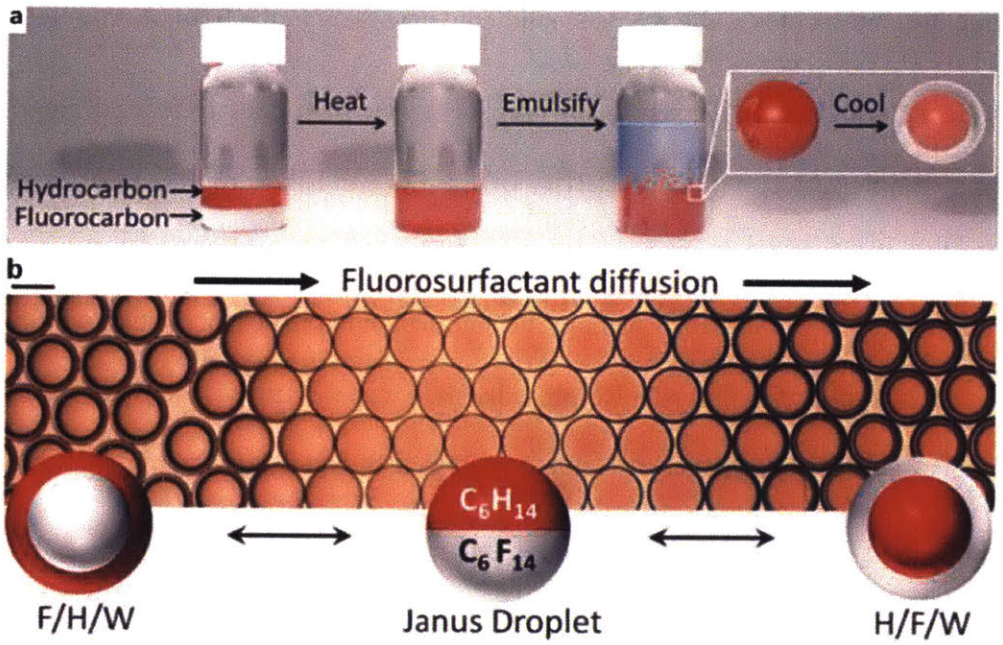

Figure 1.1 a) Complex emulsion fabrication. b) Complex emulsion morphology change with FC surfactant diffusing from left to right. Reprinted from Ref. 20 with permission. Copyright 2015, Nature Publishing Group.

In this double emulsion system, the morphology is controlled by three interfacial tensions, H-W interface, λ_H, the F-W interface, λ_F, and the F-H interface, λ_{FH}. The solvent combinations are carefully chosen such that λ_H and λ_F are significantly larger than λ_{FH}, so that the droplet morphology is determined by the relative strength of λ_H and λ_F. (**Figure 1.2**) In order to create

stable emulsions, surfactants are needed to lower the surface tension between two liquids. We use both HC surfactants (e.g., sodium dodecyl sulfate, SDS, hydrophilic head group and alkyl tail group) and FC surfactants (e.g. Zonyl-FS 300, hydrophilic head group and fluorous tail group) to tune the two interfacial tensions, HC/water and FC/water. With SDS dominant, for example, the double emulsion starts in FC-in-HC-in-water (F/H/W). Then by adding Zonyl, the morphology goes through a Janus state and ends with a HC-in-FC-in-water (H/F/W) double emulsion (**Fig 1.1b**).

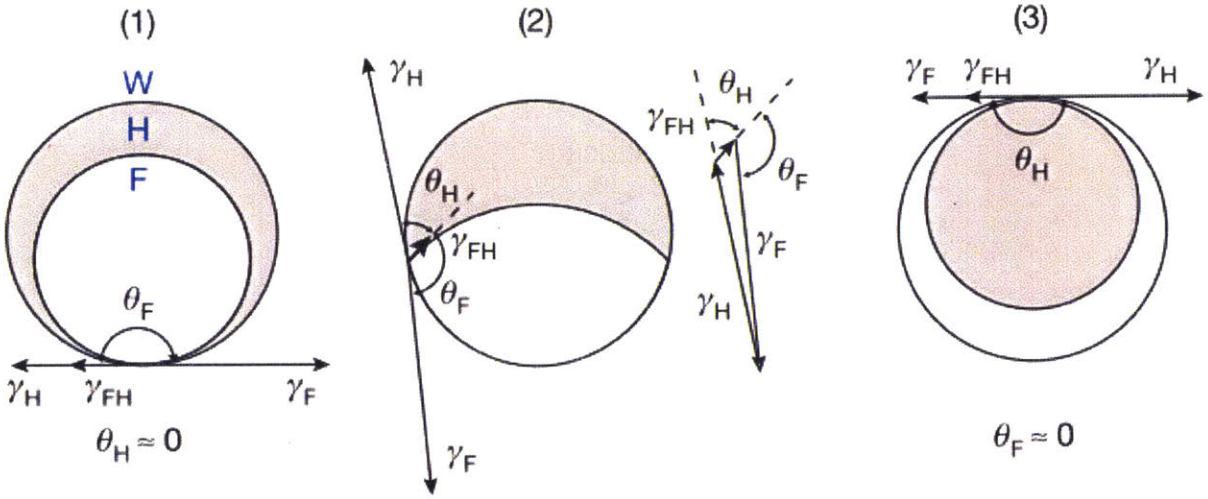

Figure 1.2. Complex emulsion morphology controlled by three interfacial tensionsλ_H, λ_F and λ_{FH}. (1) F/H/W. (2) Janus. (3) H/F/W. Copyright 2015, Nature Publishing Group.

The morphology changes are reversible, and we have shown that by using stimuli-responsive surfactants, the morphology change could be triggered by pH, light (**Figure 1.3a**),[20] or enzyme activity (**Figure 1.3b**).[21] By designing novel surfactants that respond to external stimuli, we herein propose that this dynamic complex emulsion system could be a powerful liquid-phase sensing platform for complex chemical and biological analytes such as proteins, oligonucleotides, and bacteria.

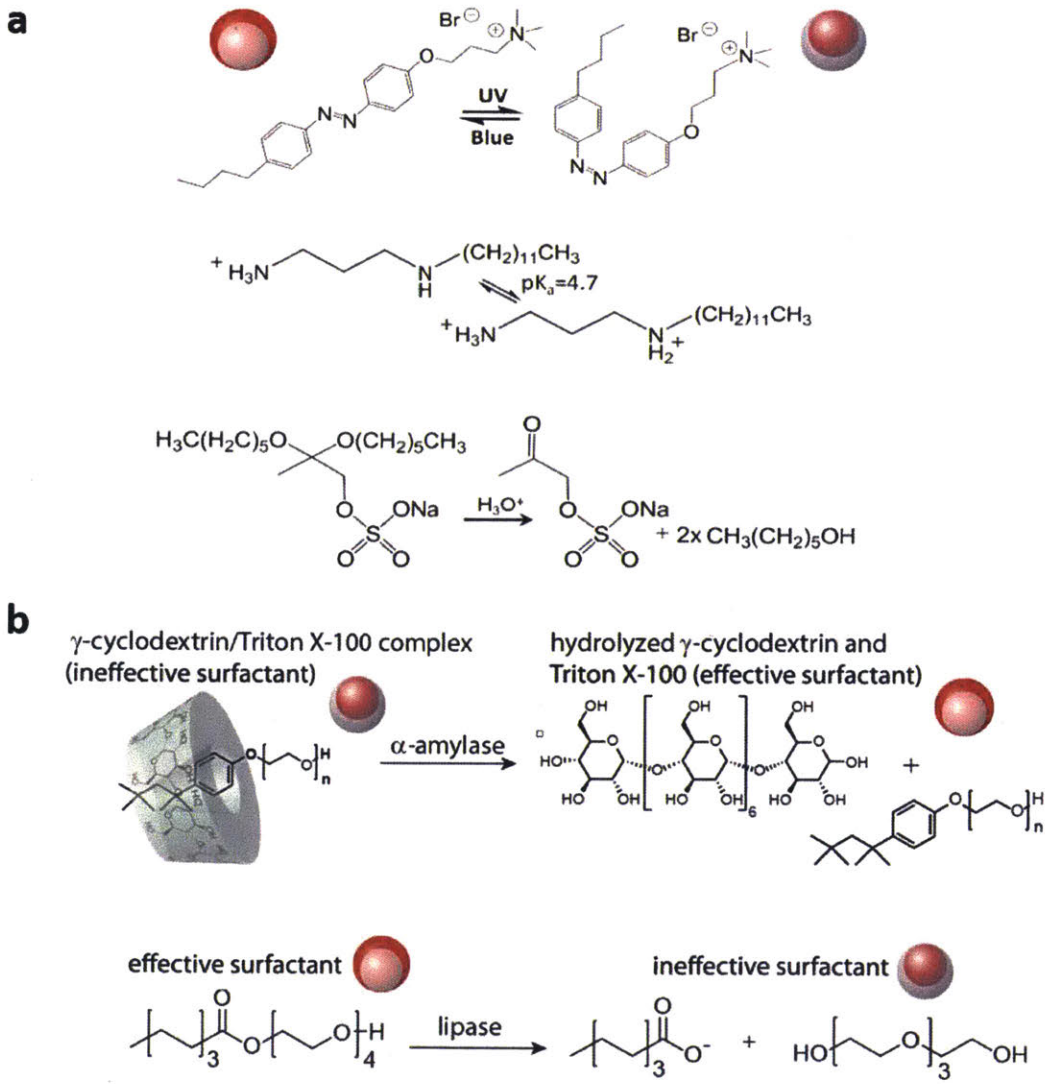

Figure 1.3. Droplet morphology change by using stimuli-responsive surfactants. a) Morphology change from F/H/W to H/F/W with light and pH. b) Morphology change with enzyme activity. Reprinted from Ref. 21. Copyright 2017, National Academy of Sciences.

Another advantage of the complex smart colloids are their intrinsic optical properties. The droplets themselves are micro-lenses. [21,22] The dynamically tunable droplets acting as micro-lenses can focus, scatter, or redirect light. **Figure 1.4a** shows a ray diagram of a droplet under different morphologies. Double emulsions at morphologies of either H/F/W or F/H/W would converge or diverge the light, respectively. The droplets are transparent at the Janus state. If a graphic picture is placed under a well of droplets, the picture will be blocked if the droplets are not at the Janus state (**Figure 1.4b**). The bi-phasic emulsion droplets can be fabricated with liquid of varying refractive indexes to display variable and controllable focal lengths. Both experimental demonstrations and wave-optical modelling have been shown to provide the fundamentals of these materials being used as display technologies and micro-scale imaging devices.[22]

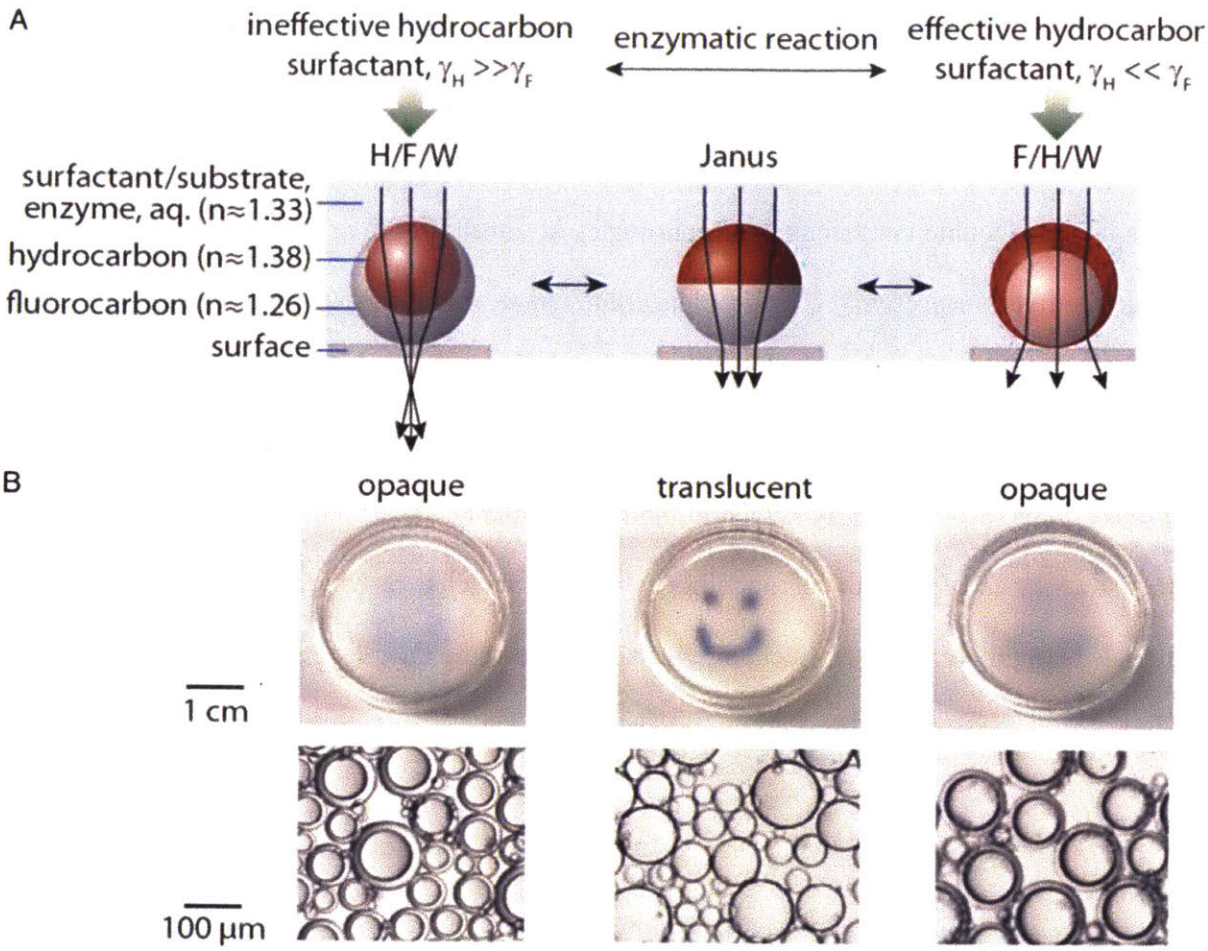

Figure 1.4. Reconfigurable droplets act as tunable lenses and the optical transmission of an emulsion film depends on the droplet morphology. a) Schematic ray diagrams of the complex droplets composed of hydrocarbon and fluorocarbon within a continuous phase of aqueous solution. b) Aligned beneath the droplet schematics are corresponding photographs of polydisperse emulsions in a Petri dish placed over an image of a smiley face to demonstrate changes in the optical transmission. Reprinted from Ref. 21. Copyright 2017, National Academy of Sciences.

1.4 Challenges and Objectives

Previous work on the complex emulsion droplets only demonstrate a proof-of-concept system for aqueous sensing using model compounds. In order for the emulsion droplets to be used as sensors in a commercial device, several problems have to be addressed. The responsive

surfactants are used in the continuous phase and will be expensive to apply in large scale real applications. A more generic surfactant platform has to be designed to bind wider types of analytes without complicated synthetic effort. A more elaborate optical mechanism need to be coupled with the molecular recognition for sensing readout. Solving these problems will transform the dynamic complex emulsions into smart colloidal assays for real applications.

This thesis focuses on exploring and expanding the emulsion droplets as assays for applications in biosensing. Both chemical/biological functionalization and transduction mechanism into digitalized signals were studied. In Chapter 2, we demonstrate an example of using emulsion agglutination assays for E.*coli* sensing with a continuous phase carbohydrate surfactant. In Chapter 3, we expand the emulsion assay using interfacial bioconjugation methods and eliminate the needs of a synthetic surfactant in the continuous phase. In Chapter 4, we develop the protein-protein agglutination assay with a thermal stable protein conjugate to the droplet-water interface for sensing of Zika protein NS1.

1.5 References

(1) Swager, T. M. Sensor Technologies Empowered by Materials and Molecular Innovations. *Angew. Chem. Int. Ed.* **2018**, 4248–4257.

(2) Kauffman, D. R.; Star, A. Carbon Nanotube Gas and Vapor Sensors. *Angew. Chem. Int. Ed.* **2008**, *47* (35), 6550–6570.

(3) Carregal-Romero, S.; Caballero-Díaz, E.; Beqa, L.; Abdelmonem, A. M.; Ochs, M.; Hühn, D.; Suau, B. S.; Valcarcel, M.; Parak, W. J. Multiplexed Sensing and Imaging with Colloidal Nano- and Microparticles. *Annu. Rev. Anal. Chem.* **2013**, *6* (1), 53–81.

(4) Jans, H.; Huo, Q. Gold Nanoparticle-Enabled Biological and Chemical Detection and Analysis. *Chem. Soc. Rev.* **2012**, *41* (7), 2849–2866.

(5) Horgan, A. M.; Moore, J. D.; Noble, J. E.; Worsley, G. J. Polymer- and Colloid-Mediated Bioassays, Sensors and Diagnostics. *Trends Biotechnol.* **2010**, *28* (9), 485–494.

(6) Elghanian, R.; Storhoff, J. J.; Mucic, R. C.; Letsinger, R. L.; Mirkin, C. A. Selective Colorimetric Detection of Polynucleotides Based on the Distance-Dependent Optical Properties of Gold Nanoparticles. *Science* **1997**, *277* (5329), 1078–1081.

(7) Chan, W. C.; Nie, S. Quantum Dot Bioconjugates for Ultrasensitive Nonisotopic Detection. *Science* **1998**, *281* (5385), 2016–2018.

(8) Phillips, R. L.; Miranda, O. R.; You, C.-C.; Rotello, V. M.; Bunz, U. H. F. Rapid and Efficient Identification of Bacteria Using Gold-Nanoparticle–Poly(para-Phenyleneethynylene) Constructs. *Angew. Chem. Int. Ed.* **2008**, *47* (14), 2590–2594.

(9) Driskell, J. D.; Jones, C. A.; Tompkins, S. M.; Tripp, R. A. One-Step Assay for Detecting

Influenza Virus Using Dynamic Light Scattering and Gold Nanoparticles. *Analyst* **2011**, *136* (15), 3083.

(10) Tokumitsu, H.; Ichikawa, H.; Fukumori, Y. Chitosan-Gadopentetic Acid Complex Nanoparticles for Gadolinium Neutron-Capture Therapy of Cancer: Preparation by Novel Emulsion-Droplet Coalescence Technique and Characterization. *Pharmaceutical research.* **1999**, pp 1830–1835.

(11) Williams, R.; Peisajovich, S. G.; Miller, O. J.; Magdassi, S.; Tawfik, D. S.; Griffiths, A. D. Amplification of Complex Gene Libraries by Emulsion PCR. *Nat. Methods* **2006**, *3* (7), 545–550.

(12) Patravale, V. B.; Mandawgade, S. D. Novel Cosmetic Delivery Systems: An Application Update. *Int. J. Cosmet. Sci.* **2008**, *30* (1), 19–33.

(13) Chen, L.; Li, Y.; Fan, J.; Bisoyi, H. K.; Weitz, D. A.; Li, Q. Photoresponsive Monodisperse Cholesteric Liquid Crystalline Microshells for Tunable Omnidirectional Lasing Enabled by a Visible Light-Driven Chiral Molecular Switch. *Adv. Opt. Mater.* **2014**, *2* (9), 845–848.

(14) Chakravarti, A. K.; Chowdhury, S. B.; Chakrabarty, S.; Chakrabarty, T.; Mukherjee, D. C. Liquid Membrane Multiple Emulsion Process of chromium (VI) Separation from Waste Waters. *Colloids Surfaces A Physicochem. Eng. Asp.* **1995**, *103* (1–2), 59–71.

(15) Utada, a S.; Lorenceau, E.; Link, D. R.; Kaplan, P. D.; Stone, H. a; Weitz, D. a. Monodisperse Double Emulsions Generated from a Microcapillary Device. *Science* **2005**, *308* (5721), 537–541.

(16) Vladisavljević, G. T.; Williams, R. A. Recent Developments in Manufacturing Emulsions

and Particulate Products Using Membranes. *Adv. Colloid Interface Sci.* **2005**, *113* (1), 1–20.

(17) Buyukozturk, F.; Benneyan, J. C.; Carrier, R. L. Impact of Emulsion-Based Drug Delivery Systems on Intestinal Permeability and Drug Release Kinetics. *J. Control. Release* **2010**, *142* (1), 22–30.

(18) Brake, J. M.; Daschner, M. K.; Luk, Y.-Y.; Abbott, N. L. Biomolecular Interactions at Phospholipid-Decorated Surfaces of Liquid Crystals. *Science.* **2003**, *302* (5653), 2094–2097.

(19) Sivakumar, S.; Wark, K. L.; Gupta, J. K.; Abbott, N. L.; Caruso, F. Liquid Crystal Emulsions as the Basis of Biological Sensors for the Optical Detection of Bacteria and Viruses. *Adv. Funct. Mater.* **2009**, *19* (14), 2260–2265.

(20) Zarzar, L. D.; Sresht, V.; Sletten, E. M.; Kalow, J. a.; Blankschtein, D.; Swager, T. M. Dynamically Reconfigurable Complex Emulsions via Tunable Interfacial Tensions. *Nature* **2015**, *518* (7540), 520–524.

(21) Zarzar, L. D.; Kalow, J. A.; He, X.; Walish, J. J.; Swager, T. M. Optical Visualization and Quantification of Enzyme Activity Using Dynamic Droplet Lenses. *Proc. Natl. Acad. Sci. U. S. A.* **2017**, *114* (15), 3821–3825.

(22) Nagelberg, S.; Zarzar, L. D.; Nicolas, N.; Subramanian, K.; Kalow, J. A.; Sresht, V.; Blankschtein, D.; Barbastathis, G.; Kreysing, M.; Swager, T. M.; Kolle, M. Reconfigurable and Responsive Droplet-Based Compound Micro-Lenses. *Nat. Commun.* **2017**, *8*, 14673.

CHAPTER 2

Janus Emulsions for the Detection of Bacteria

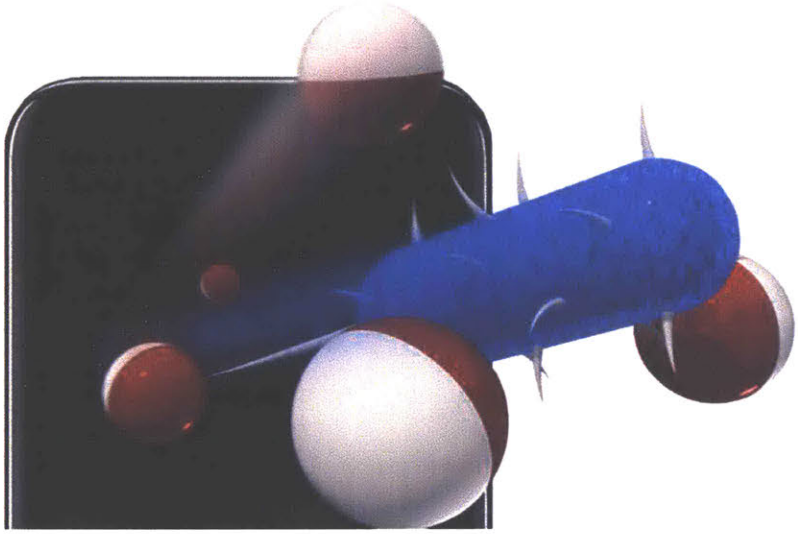

Abstract:

Janus emulsion assays that rely on carbohydrate-lectin binding for the detection of *Escherichia Coli* bacteria are de-scribed. Surfactants containing mannose are self-assembled at the surface of Janus droplets to produce particles with lectin binding sites. Janus droplets orient in a vertical direction as a result of the difference in densities between the hydrocarbon and fluorocarbon solvents. Binding of lectin to mannose(s) causes agglutination and a tilted geometry. The distinct optical difference between naturally aligned and agglutinated Janus droplets produces signals that can be detected quantitatively. The Janus emulsion assay sensitively and selectively binds to *E.coli* at 10^4 cfu/mL and can be easily prepared with long-time stability. It provides the basis for the development of inexpensive portable devices for fast, on-site pathogen detection.

Adapted and reprinted in part with permission from:

Zhang, Q.; Savagatrup, S.; Kaplonek, P.; Seeberger, P. H.; Swager, T. M. *ACS Cent. Sci.*, 2017, 3(4), pp 309-313. DOI: 10.1021/acscentsci.7b00021

Photograph Credit to Dr. Suchol Savagatrup.

Three movies can be found in the supporting information from the original online publication.

2.1 Introduction

Foodborne pathogens are a growing global public health concern. An estimated 73,000 illnesses and 60 deaths occur annually in the United States alone as a result of consuming pathogen contaminated food and water.[1] *Escherichia Coli*, for example, can be easily spread in contaminated food and water to cause serious illness and even death. In a serious 1996 *E.coli* outbreak in Japan, more than 6,000 primary schoolchildren became sick and at least 12 died;[2] while in Canada, seven of the thousands of people that fell ill died in 2000.[3] Such tragedies could have been avoided if inexpensive and fast devices to test large amounts of food and water for pathogenic bacteria prior to consumption were available. The conventional method for bacterial detection requires cell culturing and a multiday enrichment step.[4] Modern methods based on surface plasmon resonance (SPR),[5] the polymerase chain reaction (PCR),[6,7] and immunoassays[8] are much more rapid but require expensive equipment that has to be operated by trained technicians. These drawbacks of the current methods surrender the possibility of food testing before consumption. As a result, an on-site detection method that is rapid, inexpensive, and user-friendly is urgently needed.

We report an emulsion based agglutination assay for the selective and sensitive detection of bacteria. Fluid Janus droplets are powerful liquid phase sensing particles when the different hemispheres are functionalized to have orthogonal physical and biochemical properties. Janus particles with covalently modified surfaces have been used for sensing applications.[9,10] We produce liquid Janus emulsions with intrinsic functionalization by using surfactant-based recognition groups. Liquid Janus emulsions provide dynamic and compliant surfaces that mimic properties of live cells. We have targeted carbohydrate-lectin interactions that are critical to cellular recognition,[11] and utilize many weak interactions in a multivalent binding process.[12] Although a commercial agglutination assay (latex fixation assay) has been used for identifying

bacteria, it involves the functionalization of latex beads with expensive antigen or antibody and counting agglutination sites under a microscope.[13] Our emulsion assay uses the carbohydrate surfactant molecule, which self-assembles at the droplets surfaces during the emulsification process so that no further functionalization is required for bacteria recognition. Additionally, the intrinsic optical lensing behavior of the Janus droplets also enables both qualitative and quantitative detection of protein and *E. coli* bacteria. Surfactants lower the interfacial tension between two immiscible liquids and stabilize emulsion droplets. Recently, we demonstrated that stimuli-responsive surfactants can produce dynamic complex emulsions that undergo morphological switching.[14] This mechanism depends on changes in concentration or effectiveness of the surfactants and hence requires many chemical reactions to change a single droplet. In this study, we report a more sensitive transduction mechanism that does not require changes in the interfacial tensions, but rather uses the changes in the alignment of the Janus droplets for the detection of analytes. Janus morphology was maintained during the binding process and the analyte is directly visualized by the tilted Janus droplets.

2.2 Results and Discussion

Initially, we investigated the interactions between the Janus droplets and a mannose-binding lectin, Concanavalin A (ConA), which serves as a functional substitute for *E. coli* bacteria.[15] A simple mannose carrying an anomeric C-14 alkyl chain (ManC14) was designed as the surfactant and was synthesized via a modified literature method.[16] Janus emulsions, composed of equal volumes of hexane and FC-770 (a commercially available perfluoronated solvent from 3M) in aqueous continuous phase were fabricated. Both monodispersed and polydispersed droplets were used in this study. The detailed fabrication procedure and the dynamic nature of these droplets are explained in section 2.4. ManC14 and Zonyl FS300, a commercially available fluorocarbon

surfactant, were then used to stabilize the emulsion assay in the Janus morphology. The Janus emulsion assay can be prepared in large scale while maintaining the stability and sensing behavior over several month. The force of gravity aligned the denser FC-770 phase downward, leading to the spontaneous alignment of the Janus emulsions in an upright direction with the hydrocarbon phase and ManC14 on top (**Figure 2.1a**). Aligned Janus emulsions appeared as transparent simple droplets under the microscope and the internal structure was not apparent (**Figure 2.1b**). However, upon the addition of a buffered solution of ConA and gentle agitation, bound Janus droplets realigned in a unique tilted configuration with the hexane faces joined together in an agglutinated configuration (**Figure 2.1c**) within seconds. The hydrocarbon surfactant ManC14 self-assembled at the hexane/water interface to lower the interfacial tension and created an affinity for ConA on the hydrocarbon hemisphere. ConA has four mannose binding subunits (**Figure 2.1d**) and crosslinks the droplets via the hydrocarbon phase to generate the tilted (agglutinated) clusters (**Figure 2.1e**).

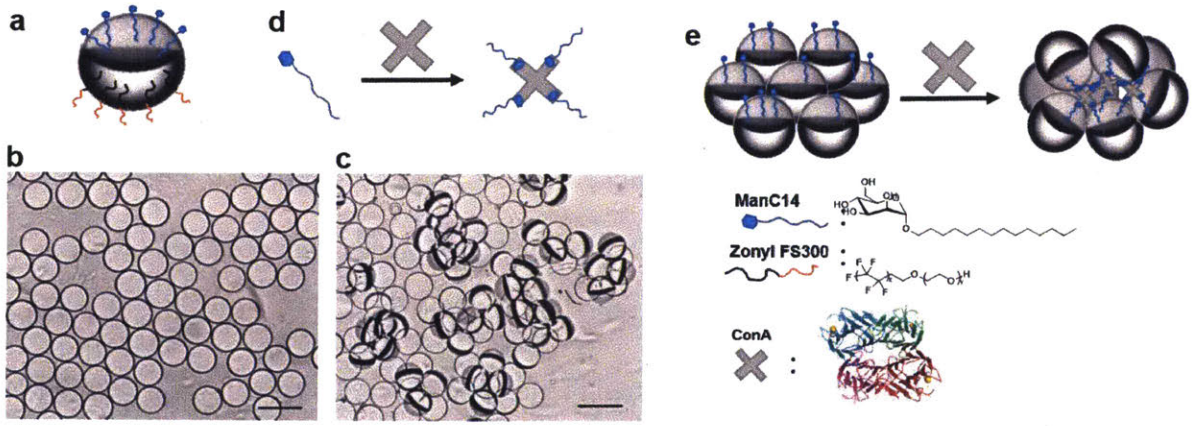

Figure 2.1. a) Side view of a Janus droplet stabilized by ManC14 and Zonyl FS 300. Optical micrographs of b) transparent pristine monodispersed Janus emulsions and c) agglutinated Janus emulsions scatter light after exposure to ConA. Scale bar 100μm. Schematic representation of Janus emulsion agglutination. d) Multivalent binding of ConA to ManC14. e) Agglutinated Janus emulsions with ConA and ManC14.

Janus emulsions can become H/F/W double emulsion when additional fluorocarbon surfactant is added. To confirm that the hexane phases of Janus droplets were connected via ConA, excess fluorocarbon surfactant Zonyl was added to the agglutinated emulsion assay to induce a morphology change from Janus to double emulsions. Under these conditions, non-agglutinated Janus emulsions transform symmetrically into double emulsions H/F/W (**Figure 2.2a, c**). However, with ConA-agglutinated Janus emulsions, the droplets maintained an asymmetric structure wherein the pre-organized ConA: ManC14 groups behaved as a persistent connective anchor to the hydrocarbon phase (**Figure 2.2 b, d** and see also a video in the Supporting Information from the original publication). Bovine serum albumin (BSA) was used as a non-mannose binding protein for the control experiments. No agglutination or significant perturbation of the optical properties was observed with even high concentration of BSA (up to 1 mg/mL, see the experimental details in section 2.4).

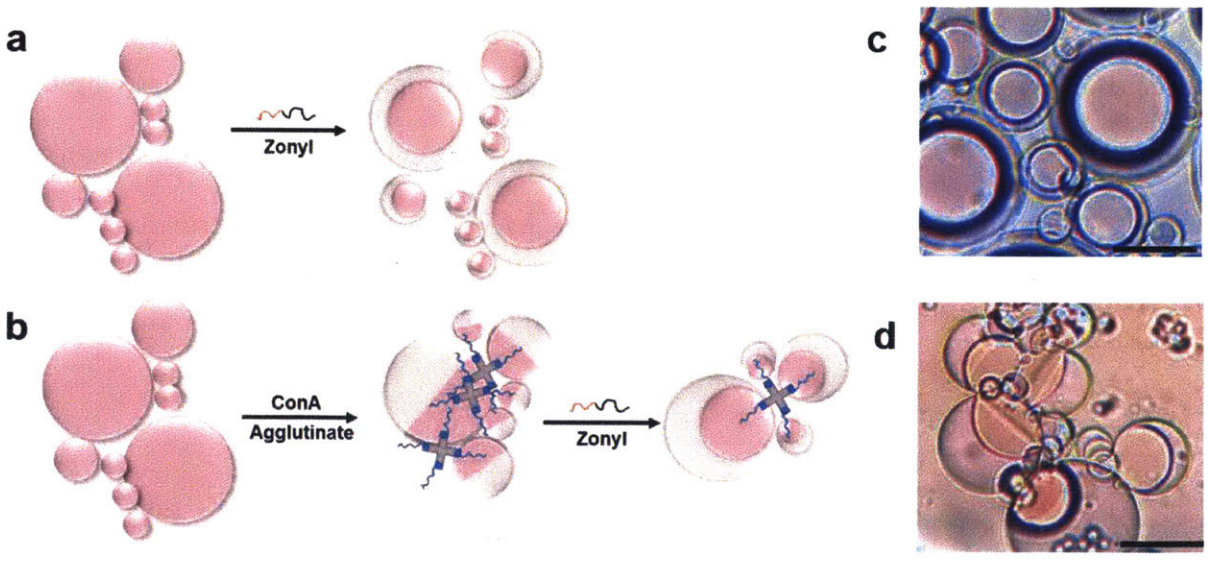

Figure 2.2. Scheme and optical images showing directional morphology change with addition of excess Zonyl surfactant. The hexane phase has been dyed in pink for display purposes. a), c) Janus emulsion change into H/F/W double emulsion. b), d) Agglutinated Janus emulsion with addition of ConA. Scale bar equals 50 μm.

Janus emulsions with the chosen fluids have compensating refractive indices which enable detection by optical transmission. Vertically aligned droplets on a horizontal surface are transparent, whereas the agglutinated droplets are highly scattering. This significant change can be easily observed by visual detection with-out any instrumentation or energy. Beyond a qualitative scattering/non-scattering assay, quantitative detection schemes are possible when image processing algorithms are employed to analyze the optical micrographs.

In an effort to create a qualitative binary assay for analytes, Janus emulsions were placed in a transparent analysis chamber that was positioned over a quick response (QR) code printed on paper (**Figure 2.3a**). Upon the addition of ConA, the Janus droplets agglutinated and the chamber became opaque, rendering the QR code unreadable by a smartphone (**Figure 2.3b**). This change occurred within less than five seconds after the addition of ConA and gentle agitation, which enables the Janus emulsion assay for a detection with instant readout. The Janus droplets behave as lens and the optical scattering is strongest at distances > 5 mm. At shorter distances, the QR code can still be scanned and the distance (D) at which the code was readable varies with ConA concentration (**Figure 2.3c**). The greater the D, the lower the concentration of ConA required to disable the QR code. As a result, binary distance dependent measurements can provide some level of quantitation.

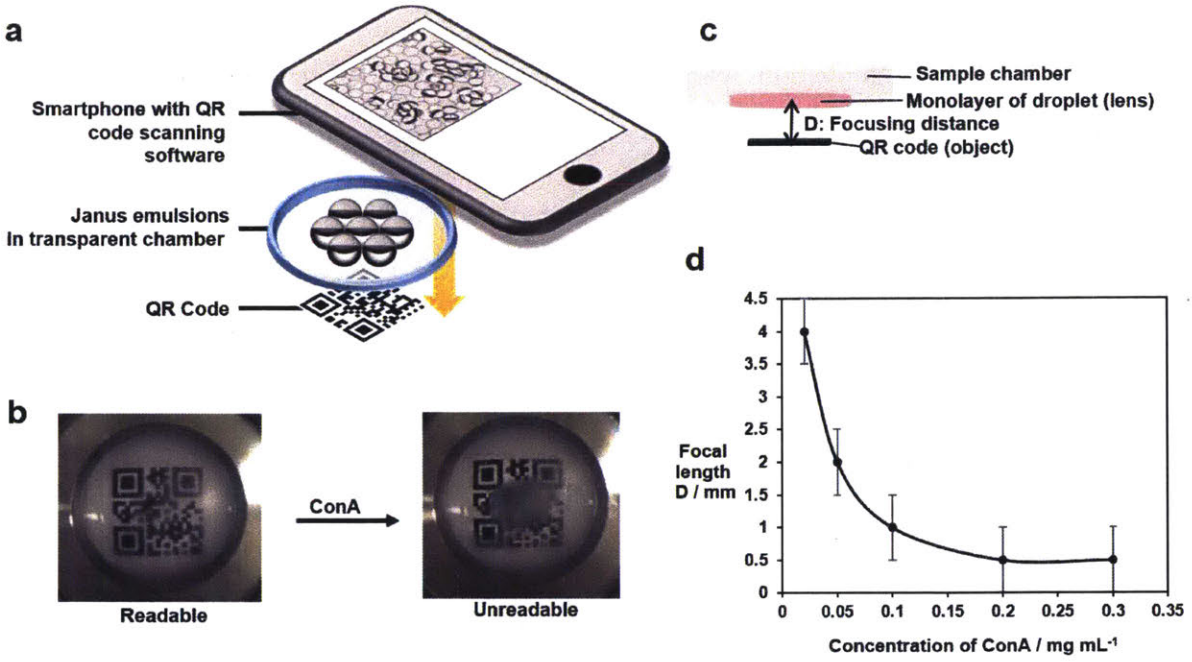

Figure 2.3. a) Schematic view of qualitative detection of the agglutinated Janus emulsions. The Janus emulsions are placed on a transparent analysis chamber. The QR code enables the binary qualitative detection of agglutination. b) Optical signal detected using a QR code before and after exposure to ConA. c) The focusing distance D, with droplet monolayer as a lens and QR code as the object. d) Correlation of the threshold ConA concentration for the binary signal with D.

To precisely quantify the degree of agglutination, we implemented an image processing program to calculate the percentage of area covered by agglutinated Janus emulsions by evaluating the differences in optical intensity of the images before and after exposure to ConA. The program uses the adaptive thresholding algorithm to distinguish areas with higher transparency (pristine Janus emulsions) from the opaque regions (agglutinated Janus emulsions) (see experimental details in section 2.4). Optical micrographs of Janus emulsions, **Figure 2.4a-c**, show that the opaque regions increase with higher concentration of ConA. The agglutination level was defined by the percentage of areas covered by agglutinated (scattering) Janus droplets (**Figure 2.4d**). Each point represents an average of multiple pictures ($N \geqslant 5$) obtained at the given concentration of ConA.

The background without addition of ConA (**Figure 2.4a**) was analyzed with the software and showed nearly zero agglutination level output. We observed a linear correlation between agglutination level and the concentration of ConA up to 150 μg mL^{-1} (**Figure 2.4d**). At higher concentrations of ConA, agglutinated droplets saturated the imaging area, and thus a plateau in the agglutination percentage was observed.

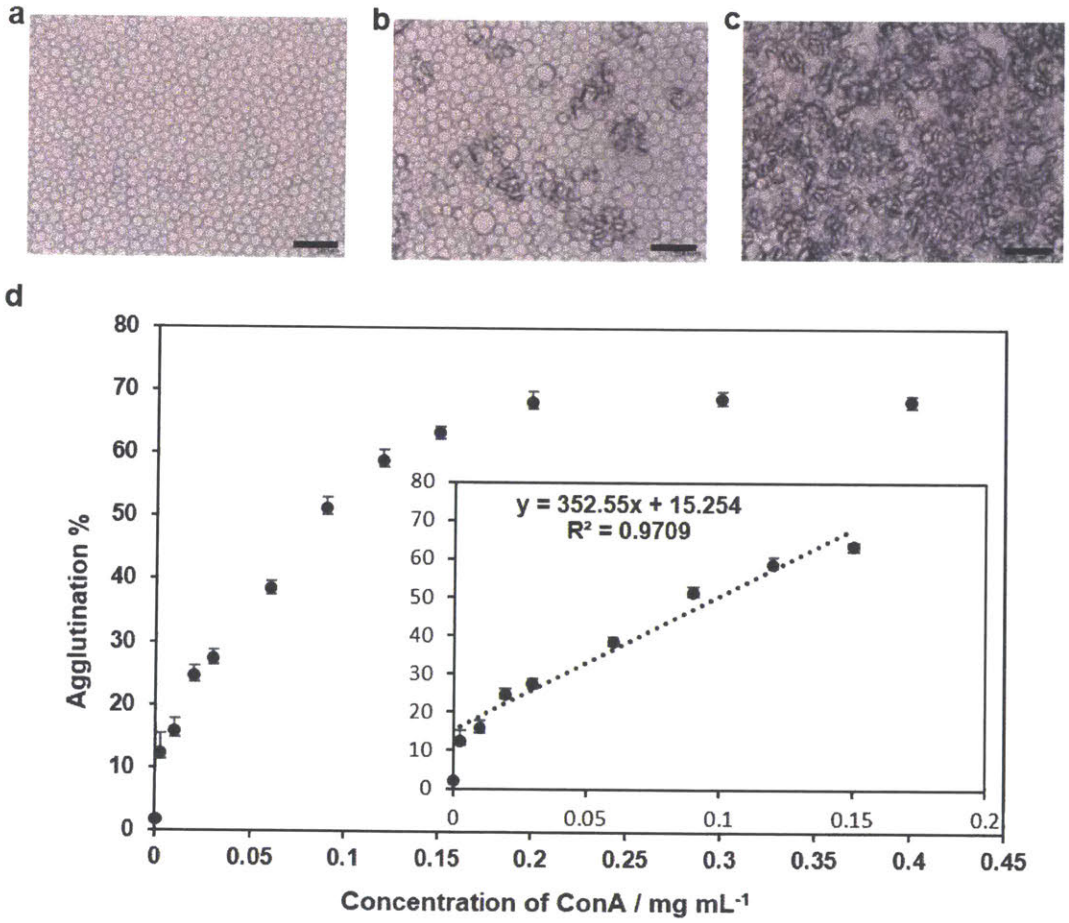

Figure 2.4. Correlation of ConA concentration and agglutination level. a) Janus emulsion without ConA. b) With 0.03 mg mL^{-1} ConA. c) With 0.12 mg mL^{-1} ConA. d) Correlation between concentration of ConA and agglutination level. Scale bar equals 250 μm.

Having established a detection scheme with the help of ConA, bacterial detection of *E.coli* ORN 178 strains was explored. These bacteria express the mannose-specific lectin, FimH, for the recognition and binding to host cells. Agglutination of droplets was observed 48 hours after incubation with live *E.coli*. Unexpectedly, a change in morphology from Janus to H/F/W double emulsions was observed in addition to agglutination (**Figure 2.5a**). Symmetric Janus droplets are produced when the ManC14 and Zonyl concentrations are adjusted such that hexane/water and FC-770/water interfacial tensions are equal. When live *E.coli* binds to ManC14, the cell appears to either reduce the effectiveness of ManC14 as surfactant at the interface or, perhaps more likely, removes some ManC14 from the droplets. The active ManC14 that was present on the surface of drop-lets may have been significantly decreased due to the high concentration of bacteria (> 10^9 cfu/mL) after 48 h of proliferation. In this case, the Zonyl stabilized FC-770/water interface had a lower interfacial tension resulting in the equilibrium morphology of the double emulsion (H/F/W). This morphological change was not observed upon the addition of ConA since the lectin itself is small and inanimate, and neither decreases the effectiveness of ManC14 nor removes it from the droplet. We speculate that the slower rate of agglutination for the emulsions with live bacteria as compared to ConA resulted from the dynamic nature of the pili that contain the FimH recognition elements.[17]

To accelerate agglutination, bacteria were fixed via 4% paraformaldehyde.[18] While maintaining the FimH binding activity, the fixed pili are static,[19] similar to ConA, and are more efficient in agglutinating droplets. Janus emulsion agglutination was observed after two hours with paraformaldehyde treated ORN178 strains. To determine the limit of detection, treated bacteria were diluted to various concentrations and agglutination was detected using a smartphone and QR code recognition for ORN 178 strains at 10^4 cfu/mL (see the Supporting Information from the

original publication for a movie on smartphone-based *E.coli* detection). It is important to note that this method is comparable in sensitivity to the existing methods for pathogen detection. The conventional plating technique can detect single bacteria but the culturing process takes several days. Other immunological and bioluminescence method as well as the nucleic acid based assays have a detection limit of 10^3-10^4 cfu/mL, but re-quire special laboratory equipment and trained technicians.[20]

As a control, ORN 208 strains, carrying a mutation in the FimH gene, that compromises the pili's ability to bind mannose, were subjected to the same tests and no agglutination was observed at the concentrations that suffice to detect ORN178 (**Figure 2.5b**, **Figure 2.5c**). Similar to the agglutination assay with ConA, agglutination was observed and the Janus morphology was maintained. A transformation to a double emulsion at these lower concentrations of fixed bacteria was not observed. We expect that this system can be further improved by employing more elaborate carbohydrate surfactants. In a real-world application, customized protocols will be necessary for sample preparation and there may be interfering effects. To address the latter we have conducted investigations with non-mannose binding protein and find that the binding is not affected by the generic protein (**Figure 2.9**).

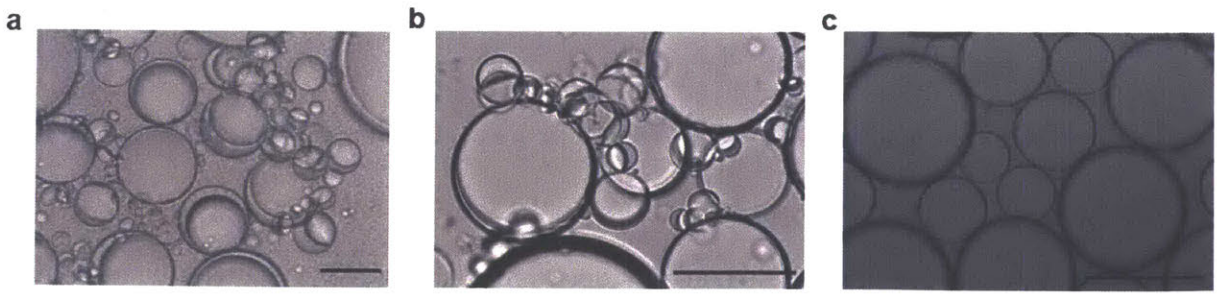

Figure 2.5. Micrographs showing emulsion agglutination with *E.coli* bacteria. a) Janus emulsions change into H/F/W double emulsion after 48 incubation with live ORN 178 *E.coli*. Agglutination is also observed. b) Janus emulsions agglutination, 2 h after 4% paraformaldehyde treated ORN

178 *E.coli* bacteria (10^4 cfu/mL) were added. c) No agglutination was observed with ORN 208 strains under the same testing conditions. Scale bar equals 100 μm.

2.3 Conclusions

In summary, we have developed a Janus emulsion agglutination assay based on carbohydrate-lectin binding. The mannose surfactant functionalized emulsion assay described in this work was designed specifically for *E.coli* as a model system. The assays can be expanded to arrays with multiple carbohydrate surfactants to differentiate various types of bacterial strains. The self-assembly of glycosylated surfactant molecules on surface of droplets provided multivalent binding sites to target analytes. We demonstrated that this agglutination detection method can be analyzed qualitatively with a QR code for a binary readout and quantitatively with designed image processing software. Both methods give results within a minute. The Janus emulsion assay allows for the detection of *E.coli* bacteria at concentration of 10^4 cfu/mL. Therefore, this method is comparable in sensitivity to the existing methods for pathogen detection. The Janus emulsion agglutination assay is a fast, inexpensive, and sensitive method that can be implemented with commercial smartphones for on-site detection of biomolecules and pathogens.

2.4 Experimental Details

General Methods and Instrumentation

Hexane, FC-770, D-(+)-Mannose, 1-tetradecanol, Concanavalin A, Bovine serum albumin and Zonyl FS-300 were purchased from Sigma-Aldrich. HEPES buffer (1 M) was purchased from ThermoFisher. Solvents were purchased from Sigma-Aldrich and used as received. NMR spectra were recorded using a Bruker Avance 400 MHz NMR spectrometer and were referenced to the proton resonances resulting from incomplete deuteration of NMR solvent (^{1}H). High resolution mass spectrum was determined with a Waters Q-TOF Micro Mass Spectrometer using electrospray

ionization (ESI) ion source. Bright-field images were taken with a Zeiss Axiovert 200 inverted microscope equipped with a Zeiss AxioCam Hrc camera.

Synthetic Procedures

ManC14 was synthesized according to a modification of a published method.[21] D-(+)-Mannose (0.75 g, 4.16 mmol) was reacted with 1-tetradecanol (10.71 g, 0.05 mol) in 1,4-dioxane (15 ml) containing 96% H_2SO_4 (40 µl) for 12 h followed by neutralization and evaporation of volatile compounds. The crude product was purified by column chromatography on SiO_2 (20% EtOH/EtOAc) to obtain the product as a while power. ^{1}H NMR (400 MHz, $CDCl_3$): δ 4.83 (s, 1H). ^{13}C NMR (400MHz, $CDCl_3$): δ 99.96, 72.12, 71.55, 71.03, 68.01, 66.13, 31.94, 29.71, 29.62, 29.43, 26.14, 22.70, 14.13. ESI-MS: calculated for $C_{20}H_{44}O_6N$ ($[M+NH_4]^+$): 394.3163, found: 394.3170. Both ^{1}H NMR and ^{13}C NMR are attached as appendix.

Janus Emulsion Assay Preparation

Janus emulsions, composed of equal volumes of hexane and FC-770 in aqueous continuous phase were fabricated using either bulk emulsification or a microfluidics device, which generates polydisperse or monodisperse droplets respectively. Both methods could generate emulsion assays applicable for qualitative and quantitative detections. Monodispersed emulsion assays were fabricated for Figure 1 for proof-of-concept experiments. However, polydisperse emulsion assays were preferentially used for later experiments because the fabrication process is easier and doesn't require specialized equipment, which is essential for our proposed on-site sensor application. In a polydisperse emulsion assay, smaller droplets tends to be tilted and stick on to the surface of bigger droplets (**Figure 2.6**). Large Janus droplets (more than 200 µm in diameter) will not tilt because the binding strength between carbohydrate surfactant and lectin does not provide enough force to

tilt the particles against gravity. Thus, we deliberately designed the Janus droplets to be in the range of 50-150 μm in diameter to facilitate the tilting motion upon agglutination. However, droplets in different sizes are all connected together with ConA and can be confirmed with the movie provided as supporting information from the original publication. Thus we observed no differences in agglutination and limits for detection for the droplets within the ranges of diameters reported.

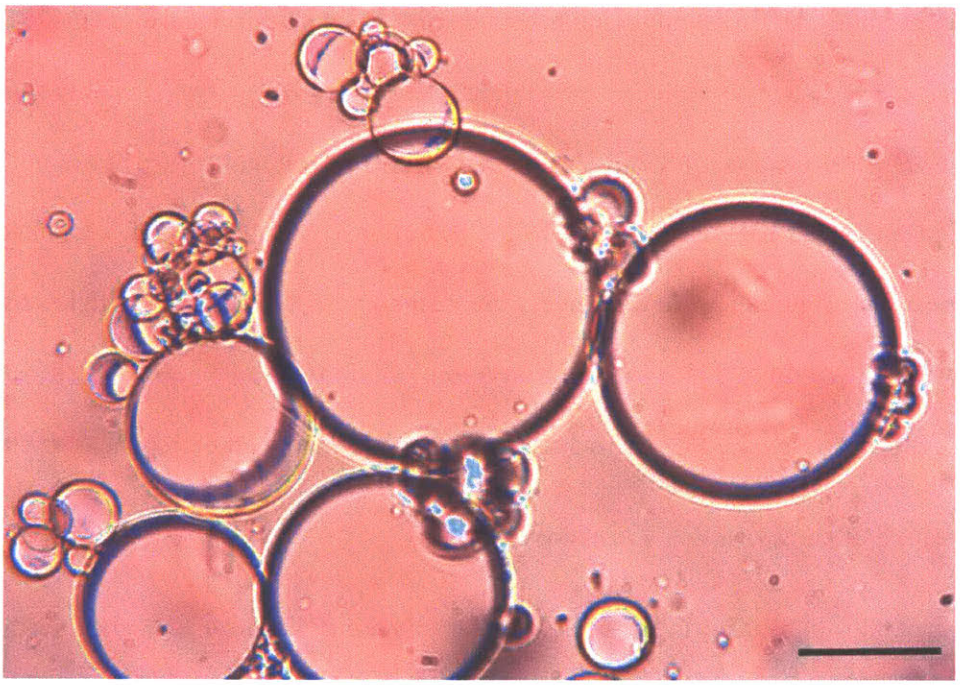

Figure 2.6. Agglutinated Janus droplets in different sizes.

In both fabrication processes, the hydrocarbon phase (hexane) and fluorocarbon phase (FC-770) were mixed and heated above the upper critical temperature to generate a single droplet phase. This droplet phase was then dispersed into the continuous aqueous phase containing the two surfactants to generate single phase emulsions and upon cooling, the hexane and FC-770 phases

separated to generate Janus emulsions. The composition of all droplets was identical because every droplet originated from the same single phase.

For the continuous water phase, two surfactants, ManC14 and Zonyl FS 300, were used to stabilize and generate the Janus emulsions. The two surfactants were dissolved in HEPES buffer solution (10 mM, containing 1 mM $CaCl_2$ and 1 mM $MnCl_2$, pH = 7.5) separately with concentration of 0.0005% and 0.01% by weight, respectively. In both bulk emulsification and microfluidics method, the final volume ratio between ManC14 solution and Zonyl FS 300 solution was kept at 1.2:1 to generate perfectly two-hemisphere Janus emulsions. Janus emulsions were loaded into a stainless steel sample holder with a 1 cm deep well and a 1.5 cm diameter viewing window. We loaded 0.5 mL of mixed surfactant solution containing 30 μL of hexane/FC-770 droplet phase into sample holder to effectively create a monolayer of Janus emulsion that covered the whole viewing window. The sample holder and solution of the Janus emulsions were kept below 20 °C, the Tc of hexane/FC-770 mixture, during the sensing and image acquisition.

Dynamic Nature of the Complex Emulsion Droplets

The Janus droplets described in this work are dynamic. The dynamic morphology change process was detailed in a previous study by our laboratory.[14] Complex emulsion droplets change their morphology from double emulsion H/F/W to Janus to F/H/W with the addition of hydrocarbon surfactant. The morphology reflects the strength and concentrations of the relative hydrocarbon and fluorocarbon surfactants. The surfactant molecule prefers to reside at the interfaces to lower interfacial tensions thus changing the morphology of droplets. In the context of this work, ManC14 is the hydrocarbon surfactant and Zonyl FS 300 is the fluorous surfactant. If the system lacks the mannose surfactant, the droplets are double emulsions with fluorous phase on the outside encapsulating the hydrocarbon phase (H/F/W, as shown in **Figure 2.7a**). Addition of

the proper amount of the mannose surfactant will transform these droplets from H/F/W to Janus droplets (**Figure 2.7b**), and excess mannose surfactant can produce F/H/W double emulsions (**Figure 2.7c**). Janus droplets were intentionally designed as a result of distinct optical behavior. The morphology (double emulsion or Janus) is the direct evidence that the mannose surfactant is active in stabilizing the water/hydrocarbon interface in the Janus particles and is also the anchor for agglutination of droplets binding to the lectin ConA.

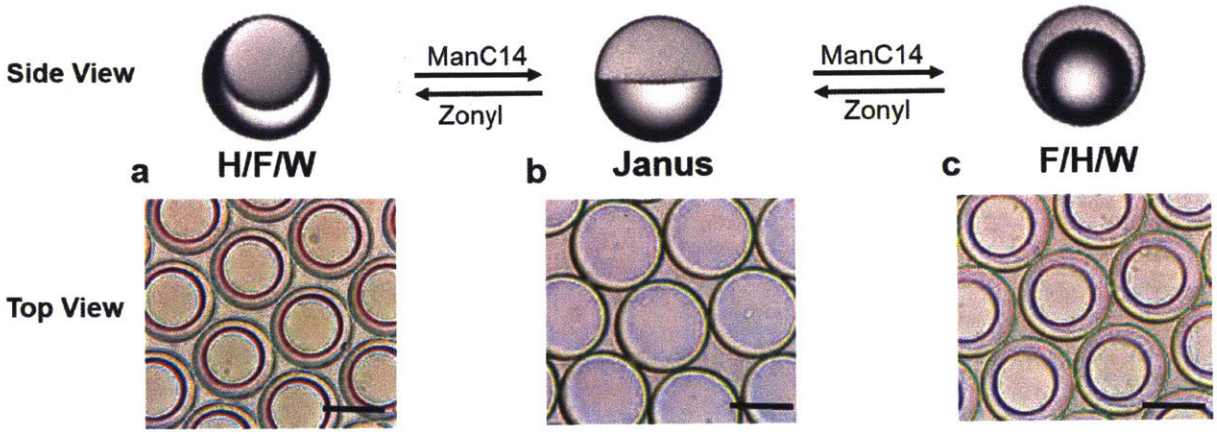

Figure 2.7. Dynamic complex emulsion droplets. a) H/F/W double emulsion in 0.01% Zonyl FS300 solution. b) Janus emulsion in solution of 0.0005% ManC14:0.01% Zonyl = 6:5 (v:v). c) F/H/W double emulsion in 0.0005% ManC14 solution. Scale bars: 50μm.

Bulk Emulsification for Polydispersed Janus Emulsions

To generate Janus emulsions via bulk emulsions, we began by preparing an equal-mixture of hexane and FC-770 with a total volume of 1 mL in a 5 mL glass vial. The mixture initially formed an immiscible solution at room temperature. The vial containing the mixture was then heated to above the Tc (20 °C) using a standard heat gun until the mixture is miscible. In another 5 mL glass vial, 1 mL of the continuous phase containing surfactants was also heated to the same

temperature as the vial containing hexane/FC-770 mixture. This precaution will mitigate the phase segregation of hexane and FC-770 upon addition before emulsification. 50 μL of heated and miscible hexane/FC-770 mixture was then injected into the heated continuous phase via a pipette. The Janus emulsions were then generated by shaking the vial using a vortex mixer at 3000 RPM for 5 seconds. The solution of emulsions was then cooled down below Tc using an ice bath. This method of bulk emulsification generated polydispersed droplets with diameters ranging from 30 to 200 μm as observed by an optical microscope.

Generation of Monodispersed Janus Emulsions via Microfluidics

Focused Flow Droplet Generator chip (channel width = 100 μm, channel depth = 20 μm, tip width = 10 μm, glass) from Micronit was used to generate monodispersed droplets. Harvard Apparatus PHD Ultra syringe pumps were used to inject the outer phase (continuous phase) and inner phase (droplet phase). The flow rates were 50 μL min^{-1} for the continuous phase and 30 μL min^{-1} for the droplet phase. The microfluidic setup was heated above the Tc of the inner phase solution using a heat lamp. Janus emulsions were then cooled below Tc to induce phase separation. The average diameter of the monodispersed droplets generated from this setup were 60 ± 10 μm.

ConA Sensing

Monodispersed or polydispersed Janus emulsions used for sensing experiments were fabricated using methods described above. ConA was dissolved in HEPES buffer solution (10 mM, containing 1 mM $CaCl_2$ and 1 mM $MnCl_2$, pH = 7.5) with various concentrations and used as the analyte. 10 μL of ConA solution was added using a micropipette to the sample holder containing Janus emulsions. Solution was then swirled gently and agglutination of Janus emulsions were observed within seconds.

A control experiments for specificity was performed in the presence of free mannose. ConA was pre-incubated with 1 mM D-(+)-Mannose in HEPES buffer (10 mM, containing 1 mM $CaCl_2$ and 1 mM $MnCl_2$, pH = 7.5) for 30 min before injected into the Janus emulsion assay. The pre-incubation of ConA with mannose inhibits the binding of ConA to the Mannose functionalized Janus Droplets and agglutination was not observed (Concentration of ConA tested in the range of 0.01-0.2 mg mL^{-1}).

For the morphology conversion experiment in the presence of agglutination, 100 μL of 5 wt% Zonyl FS 300 solution was added to the sample holder after Janus droplets were agglutinated with addition of 10 μL of 1 mg/mL ConA solution. The movie is recorded in real time to show the forced morphology change by adding excess amount of fluorous surfactant. A control experiment with Triton X-100 as the hydrocarbon surfactant was performed for comparison. 0.01% Triton X-100 and 0.01% Zonyl in volume ratio of 5:1 was used to make a control sample of Janus emulsion assay. The same amount of ConA was added and no agglutination was observed. 100 μL of 5 wt% Zonyl FS 300 solution was added to the control assay and the morphology change was symmetrical as shown in the movie.

We performed the qualitative analysis using the QR code from unmagnified images taken from the smartphone. The distance from the phone to the analysis chamber containing the Janus emulsions was approximately 10 cm. The exact distance was calibrated by the image processing software by using the known dimension of the QR code (1 cm × 1 cm). The binary response we measured was whether the QR code could be read via the software. If the QR code is readable, the Janus emulsions are not agglutinated, and vice versa.

For quantitative analysis, images were recorded before and after adding ConA solution using an inverted microscope with 4x magnification. The image processing software then pre-

processed the captured images by transforming them into greyscale images and adjusting the brightness and contrast to the reference image of blank analysis chamber. Using the pre-processed images of 4× magnification, the program first applied the adaptive thresholding algorithm to distinguish the darker edges of the Janus emulsions from the droplet complexes with tilted particles. More specifically, the program ignores the edges of the droplets that have inherent low-light intensity and only seeks the area of droplet complexes. We then set a threshold that areas with light intensity of less than 45% of the brightest regions will be considered part of the droplets complex. From this information, the area occupied by the droplet complexes was then calculated (**Figure 2.8**).

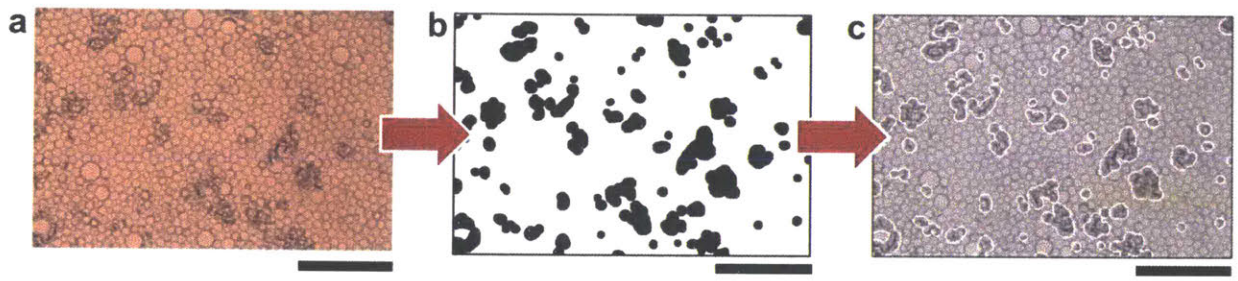

Figure 2.8. Algorithm for image analysis. The image processing program evaluated the raw image (a) by applying adaptive thresholding algorithm to distinguish area with higher transparency from opaque regions (b). The final locations of the agglutination were highlighted (c). Scale bars: 500 μm.

Generic Protein Perturbation Experiment

ManC14 functionalized Janus emulsion assay with the addition of non-mannose binding protein bovine serum albumin (BSA). 10 μL of BSA solution (in comparable concentration with ConA) was added using a micropipette to the sample holder containing Janus emulsions. The final concentration of BSA is 0.02, 0.12 and 1 mg/mL. No emulsion agglutination was observed even after extended time period. Additionally, the existence of BSA will not affect the binding between

ConA and the Janus emulsions. The agglutination behavior using ManC14 emulsion assay with ConA, BSA and ConA with the existence of BSA is shown in **Figure 2.9**.

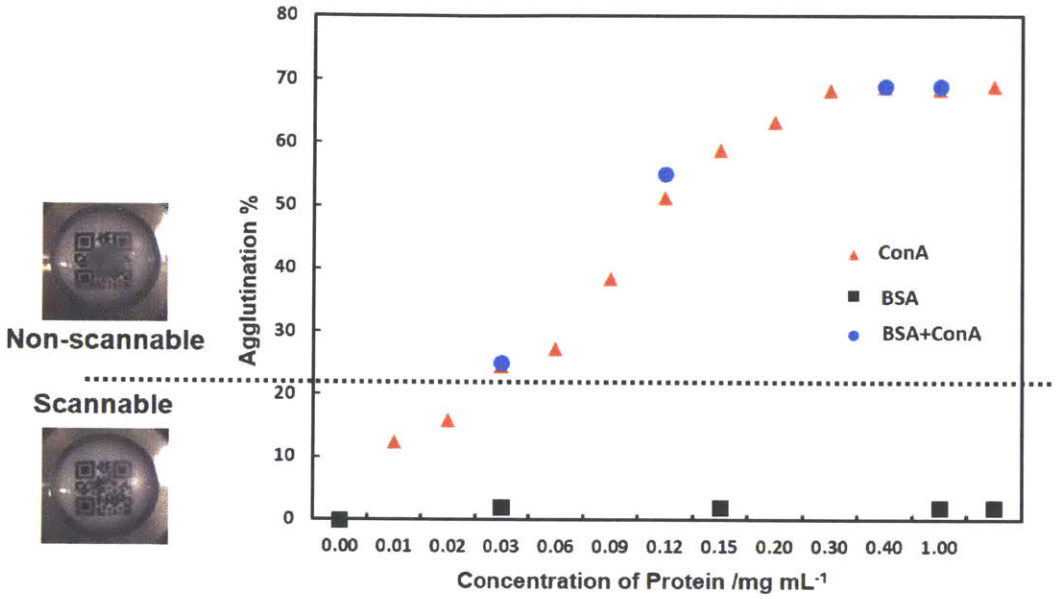

Figure 2.9. Agglutination behavior of ManC14 emulsion assay with two proteins ConA and BSA. Agglutination valued with QR code detection method.

E.coli Sensing

Bacterial strain bearing a mannose-binding protein (ORN 178) and a mutant strain lacking the mannose binding domain (ORN 208) were grown in LB media overnight at 37 °C until they reached an approximate OD 600 of 1.0 (10^8 cells). The culture was then centrifuged and cells washed twice with HEPES buffer. Live *E.coli* test was conducted by adding a 10 μL aliquot of these cells to the Janus emulsion assay. The mixture was incubated for 48 h at 37 °C before agglutination was observed under microscope.

To speed up the agglutination, both ORN 178 and ORN 208 strains were centrifuged and suspended with 4% paraformaldehyde for 1 h. The suspension is then centrifuged to pellet the cells. The supernatant solution containing paraformaldehyde was discarded, and the cells were washed three times with HEPES buffer. The bacteria was then diluted to various concentration for testing. A 10 μL aliquot of these treated cell suspension was each added to Janus emulsion assay followed by 2 h with robotic shaking under room temperature (25 °C).

Discrimination between the targeted strain, ORN 178, and the control strain, ORN 208, using a smartphone and QR code detection method is shown in a video provided in the Supporting Information from the original publication. Agglutination was also observed under a microscope (**Figure 2.5**) to confirm that agglutination is responsible rendering QR code unscannable. Janus emulsion assays without ManC14 (Triton X100 was used as hydrocarbon surfactant) will not agglutinate.

In the video of *E.coli* sensing test, a control experiment was carried out using ManC14 emulsion assay with buffer. Tests with ORN 178 and ORN 208 strains used the exact same ManC14 emulsion assay.

2.5 References

(1) Frenzen, P. D.; Drake, A.; Angulo, F. J.; Group, E. I. P. F. W.. Economic Cost of Illness due to *Escherichia Coli* O157 Infections in the United States. *J. Food Prot.* **2005**, 68 (12), 2623–2630.

(2) Watanabe, Y.; Ozasa, K.; Mermin, J. H.; Griffin, P. M.; Masuda, K.; Imashuku, S.; Sawada, T. Factory Outbreak of *Escherichia Coli* O157:H7 Infection in Japan. *Emerg. Infect. Dis.* **1999**, 5 (3), 424–428.

(3) O'Connor, D. R. Part One: *A Summary Report of the Walkerton Inquiry;* Ontario Ministry of the Attorney General Press: Ontario, **2002**, pp 1-35.

(4) Doyle, M. P.; Buchanan, R. L. *Food Microbiology: Fundamentals and Frontiers,* 4th ed.; American Society for Microbiology Press: Washington, DC, **2012**.

(5) Bhunia, A. K. Biosensors and Bio-Based Methods for the Separation and Detection of Foodborne Pathogens. *Adv. Food Nutr. Res.* **2008**, 54, 1–44.

(6) McKillip, J. L.; Jaykus, L.-A.; Drake, M. Influence of Growth in a Food Medium on the Detection of *Escherichia Coli* O157: H7 by Polymerase Chain Reaction. *J. Food Prot.* **2002**, 65 (11), 1775–1779.

(7) Nakano, S.; Kobayashi, T.; Funabiki, K.; Matsumura, A.; Nagao, Y.; Yamada, T. PCR Detection of Bacillus and Staphylococcus in Various Foods. *J. Food Prot.* **2004**, 67 (6), 1271–1277.

(8) Notermans, S.; Wernars, K. Immunological Methods for Detection of Foodborne Pathogens and Their Toxins. *Int. J. Food Micro-biol.* **1991**, 12 (1), 91–102.

(9) Yoshida, M.; Roh, K. H.; Mandal, S.; Bhaskar, S.; Lim, D.; Nandivada, H.; Deng, X.; Lahann, J. Structurally Controlled Bio-Hybrid Materials Based on Unidirectional Association of Anisotropic Micro-particles with Human Endothelial Cells. *Adv. Mater.* **2009**, 21 (48), 4920–4925.

(10) Suci, P. A.; Kang, S.; Young, M.; Douglas, T. A Streptavidin-Protein Cage Janus Particle for Polarized Targeting and Modular Functionalization. *J. Am. Chem. Soc.* **2009**, 131 (26), 9164–9165.

(11) Lis, H.; Sharon, N. Lectins: Carbohydrate-Specific Proteins That Mediate Cellular Recognition. *Chem. Rev.* **1998**, 98 (2), 637–674.

(12) Grünstein, D.; Maglinao, M.; Kikkeri, R.; Collot, M.; Barylyuk, K.; Lepenies, B.; Kamena, F.; Zenobi, R.; Seeberger, P. H. Hexameric Supramolecular Scaffold Orients Carbohydrates to Sense Bacteria. *J. Am. Chem. Soc.* **2011**, 133, 13957–13966.

(13) Weinberg, G. A.; Storch, G. A. Preparation of Urine Samples for Use in Commercial Latex Agglutination Tests for Bacterial Antigens. *J. Clin. Microbiol.* **1985**, 21 (6), 899–901.

(14) Zarzar, L. D.; Sresht, V.; Sletten, E. M.; Kalow, J. a.; Blankschtein, D.; Swager, T. M. Dynamically Reconfigurable Complex Emulsions via Tunable Interfacial Tensions. *Nature* **2015**, 518 (7540), 520–524.

(15) Huang, C. C.; Chen, C. T.; Shiang, Y. C.; Lin, Z. H.; Chang, H. T. Synthesis of Fluorescent Carbohydrate-Protected Au Nanodots for Detection of Concanavalin A and *Escherichia Coli*. *Anal. Chem.* **2009**, 81 (3), 875–882.

(16) Adasch, V.; Hoffmann, B.; Milius, W.; Platz, G.; Voss, G. Preparation of Alkyl α- and ß-D-Glucopyranosides, Thermotropic Properties and X-Ray Analysis. *Carbohydr. Res.* **1998**, 314 (3–4), 177–187.

(17) Thanassi, D. G.; Bliska, J. B.; Christie, P. J. Surface Organelles Assembled by Secretion Systems of Gram-Negative Bacteria: Diversity in Structure and Function. *FEMS Microbiol. Rev.* **2012**, 36 (6), 1046-1082.

(18) Chao, Y.; Zhang, T. Optimization of Fixation Methods for Observation of Bacterial Cell Morphology and Surface Ultrastructures by Atomic Force Microscopy. *Appl. Microbiol. Biotechnol.* **2011**, 92 (2), 381–392.

(19) Yago, T.; Leppänen, A.; Carlyon, J. A.; Akkoyunlu, M.; Karmak-ar, S.; Fikrig, E.; Cummings, R. D.; McEver, R. P. Structurally Distinct Requirements for Binding of P-selectin Glycoprotein Ligand-1 and Sialyl Lewis x to *Anaplasma phagocytophilum* and P-selectin *J. Biol. Chem.* **2003**, 278 (39), 37987.

(20) Mandal, P. K.; Biswas, A. K.; Choi, K.; Pal, U. K. Methods for Rapid Detection of Foodborne Pathogens: An Overview. *Am. J. Food Technol.* **2011**, 6(2), 87–102.

(21) Adasch, V.; Hoffmann, B.; Milius, W.; Platz, G.; Voss, G. Preparation of Alkyl α- and ß-D-Glucopyranosides, Thermotropic Properties and X-Ray Analysis. *Carbohydr. Res.* **1998**, 177-187.

CHAPTER 3

Interfacial Bioconjugation on Emulsion Droplet for Biosensors

Abstract:

Interfacial bioconjugation methods are developed for intact liquid emulsion droplets. Complex emulsion droplets having internal hydrocarbon and fluorocarbon immiscible structured phases maintain a dynamic interface for controlled interfacial reactivity. The internal morphological change after binding to biomolecules is readily visualized and detected by light transmission, which provides a platform for the formation of inexpensive and portable bio-sensing assays for enzymes, antibodies, nucleic acids and carbohydrates.

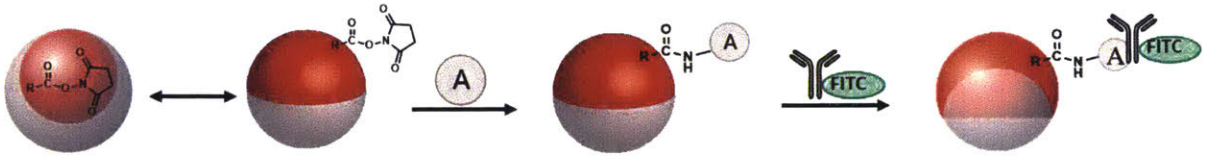

Adapted and reprinted in part with permission from:

Zhang, Q., Scigliano, A., Biver, T., Pucci, A., Swager, T.M., Interfacial Bioconjugation on Emulsion Droplet for Biosensors, *Bioorganic & Medicinal Chemistry* (2018), DOI: https://doi.org/10.1016/j.bmc. 2018.04.020

3.1 Introduction

Biosensors play an important role in medical sciences and drug discovery, with applications in healthcare, pharmaceuticals, food safety and environmental monitoring.[1,2] Biosensors take on many forms and the selectivity can be enzyme-based,[3] tissue-based,[4] antibody-based,[5] and/or DNA-based.[6] However, central to all biosensors is the need for a transduction mechanism coupled to the recognition. Electrochemical,[7,8] piezoelectric,[9] or fluorescent[10] signals are attractive because they can be quantitatively detected with inexpensive, compact equipment and do not necessarily require complicated labelling processes. There has not been uniform success in meeting these latter goals and current biosensors have limitations preventing large scale applications wherein high speed and analysis of unprocessed samples are required, such as on-site real-time environmental monitoring and food pathogen detection.

We report herein a method for interfacial functionalization on dynamic complex emulsion droplets for biosensing applications. We have identified dynamic complex emulsion droplets as powerful liquid sensing particles that can be manufactured in large scale and display intrinsic optical properties for the creation of large sensing signals. These properties stem from changes in interfacial tensions or analyte induced organizations of droplets. The first was initially explored with stimulus-responsive surfactants that give dynamic complex emulsions capable of undergoing morphological switching.[11] Using pathogen induced changes in the directional alignment of carbohydrate functionalized emulsion droplets, we have reported smartphone detection of *E.coli*.[12] To expand the utility of emulsion droplets assays for the detection of other biomolecules/organisms, expanded method for the integration of recognition or transduction functionality into these systems is needed. One issue is that the general production of precision liquid colloids is carried out by dispersing water insoluble liquids into water containing surfactants that assemble spontaneously

at the interface. Hence, to create new generations of functional interfaces, new methods are needed. To this end we have identified trialkylgallic acid (GA) groups as synthetically accessible reactive anchors and have combined these groups with well-known bio-functional schemes based upon N-hydroxysuccinimide (NHS) for amines and maleimide (MA) for thiols. A unique challenge in the functionalization of complex liquid emulsion droplets is to affect transformation of morphologies while preserving the overall structural integrity of individual droplets. This delicacy is however a key advantage of liquid colloids that maintains dynamic and compliant surfaces that mimic the properties of natural live cells. The intrinsic morphology-dependent optical properties of emulsion droplets[13] enable optical biosensors without fluorescent labelling of the target analytes. By design the emulsions are stable under the sensing conditions and we seek to create assays for bacteria, enzymes, antibodies and DNAs that can be used without the need of complex and specialized equipment.

3.2. Emulsion Assays and Surfactants Design

3.2.1. Dynamic complex emulsions

Complex emulsions are fabricated at temperatures above the upper critical solution temperature of the internal phases to create materials with precisely determined compositions.[11] Specifically, droplets containing equal volume of hydrocarbon (diethylbenzene) and fluorocarbon (HFE 7500) liquid are emulsified around 40 °C, which is above T*c* (37 °C) in an aqueous continuous phase containing Zonyl FS-300 (hereafter 'Zonyl'), which is a nonionic fluorosurfactant. Surfactants lower the interfacial tension between two immiscible liquids and stabilize emulsion droplets. Droplets containing both hydrocarbon and fluorocarbon will switch morphologies between H/F/W (hydrocarbon-in-fluorocarbon-in-water), Janus, and F/H/W

(fluorocarbon-in-hydrocarbon-in-water), with changes in the relative strength of the fluorocarbon and hydrocarbon surfactants (**Scheme 3.1**).

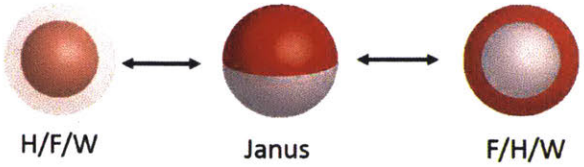

Scheme 3.1. Dynamic complex emulsions morphology change. The red phase is the hydrocarbon oil and the grey phase is the fluorocarbon oil. The color is used hereafter only for display purpose. From left to right, showing the increased strength of hydrocarbon surfactant or the decreased strength of fluorocarbon surfactants. H/F/W as in hydrocarbon-in-fluorocarbon-in-water and F/H/W as in fluorocarbon-in-hydrocarbon-in-water.

3.2.2 Surfactant design

Creating surfactant molecules that interact with analytes is the key to create couplings to droplet morphology and orientation. The orientation in the absence of perturbation is typically controlled by the density differences of the internal phases and gravity. The droplets are dynamic lenses and both morphology and orientation produce large optical signals. In our previous studies, we created assays that transduce enzymatic modification of designer surfactants[14] and the binding of bacteria and proteins to carbohydrate surfactants.[12] Optical transduction in these cases makes use of the light transparency because vertically aligned Janus droplets with internal phases having specific refractive indices. A transparency to highly scattering state is triggered by small distortions in droplet morphology or agglutination (tilting).[13] To extend these methods, we detail herein a generic surfactant platform, shown in **Scheme 3.2**, for droplet bioconjugation with proteins, nucleic acids, and carbohydrates. The three alkyl chains in the tridodecyl gallic acid shown (GA12OH) provide for a robust hydrophobic anchor and the carbonyl based functional site provides for bioconjugation. We also show that the gallic structure is an intrinsic surfactant molecule that provides sufficient stability to prevent speciation of the generic reactive droplets.

This design builds on the observation that aromatic rings with peripheral alkane chains organize at the oil-water interfaces to enhance the effectiveness at lowering interfacial tensions.[15]

To validate the interfacial behavior of the gallic derived surfactant, emulsions with and without GA12OH in the hydrocarbon oil phase were produced in the same continuous phase (0.01 wt% Zonyl in PBS buffer). The pristine emulsion droplets without GA12OH, are in double emulsion morphology (**Scheme 3.1**, H/F/W), namely hydrocarbon-in-fluorocarbon-in-water, whereas the emulsion droplets with 10 mg/mL GA12OH dissolved in the hydrocarbon phase appear in Janus configuration (**Scheme 3.1,** Janus). These results confirm that GA12OH is a good surfactant that lowers the surface tension at the oil/water interface. Aside from helping with the control droplet formation, this feature indicates that the carboxylic acid groups are presented at the aqueous interface for chemical modification.

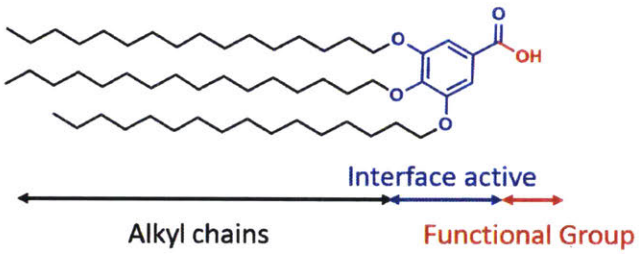

Scheme 3.2. Structures of GA12OH surfactant with three segments.

3.3. Emulsion assays for bioconjugation

3.3.1. Interfacial functionalization on emulsion droplets

After confirming the surfactant behavior of GA12OH, the chemical reactivity at the droplet interface was studied using the EDC/NHS coupling reaction. As shown in **Scheme 3.3a**, GA12OH was loaded into the droplet phase and the droplets adopted a Janus morphology. EDC and NHS solutions were then added in the continuous phase. Fluoresceinamine was used as a model reactant

for biomolecules bearing amine groups, and upon addition to the water phase reacts with the *in situ* generated NHS ester. The unreacted fluoresceinamine in the continuous water phase is removed by washing the droplets and a bright green fluorescence was observed at the hydrocarbon-water interface with confocal microscopy. The localized green fluorescence is attributed to the fluoresceinamine-NHS reaction to form a covalent amide bond at the droplet interface.

Another dye, Sulfo-Cyanine 3 amine is separately functionalized to the droplet surface using the same method described above. When two batches of droplets functionalized with different dyes were combined together, no sign of mixing dyes was observed under microscopy even after extended period of time. This further confirms the covalent bond formation at the hydrocarbon-water interface and that we can produce droplets that do not fuse or transfer functional groups between them. This latter feature is particularly important for multiplexed detection schemes.

3.3.2. GA12-NHS assay for amine conjugation

To investigate the scope of interfacial functionalization, surfactant GA12-NHS was pre-synthesized and dissolved in the droplet hydrocarbon phase (**Scheme 3.3b**). Trifluoroethanol was added to the hydrocarbon and fluorocarbon droplet phase to lower the upper critical mixing temperature. After droplets are formed in the water phase, trifluoroethanol partitions into the continuous phase and internal phases then undergo phase separation to produce double emulsions. We expect that the GA12-NHS has some partitioning to hydrocarbon-water interface as a result of its surfactant behavior. The continuous phase was exchanged twice to remove the trifluoroethanol. This is facilitated because the droplets are denser than water and remain on the bottom of flask. The continuous phase solvent exchange does not affect the stability nor the morphology of the droplets. We find that fluoresceineamine functionalization with pre-synthesized GA12-NHS has a

higher yield and resulted in 50% more intense fluorescence under confocal microscopy relative to an internal dye reference (described in section 3.5). As a result, GA12-OH and *in situ* NHS formation is not quantitative.

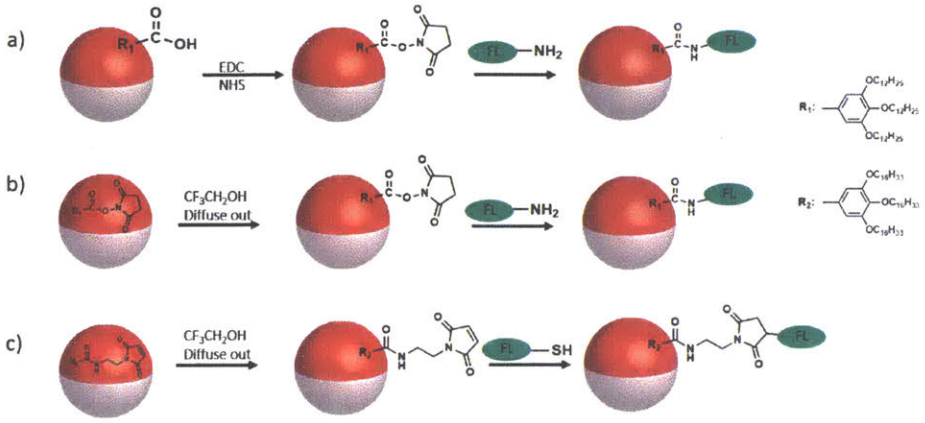

Scheme 3.3. Interfacial functionalization on the Janus droplet. The red phase is the organic oil and the gray phase is the fluorinated oil. a) *In situ* formation of GA12-NHS at droplet interface and subsequent amine conjugation. b) Pre-synthesized GA12-NHS was dissolved in the droplet hydrocarbon phase and preferably located at the hydrocarbon-water interface after trifluoroethanol diffuses out to the continuous phase, followed by interfacial amine conjugation. c) Pre-synthesized GA16-MA for interfacial thiol conjugation. FL in the schemes indicates generic fluorophores.

3.3.3. GA16-MA assay for thiol conjugation

To implement a maleimide-thiol bioconjugation scheme, GA16-MA (**Scheme 3.3c**) was pre-synthesized and loaded into the droplets. The longer hexadecyl chains were needed to increase the surfactant GA16-MA solubility in hydrocarbon phase. BODIPY-FL-Cysteine was used as the reactive model compound for biomolecules bearing thiol groups. Upon addition (**Scheme 3.3c**), this dye was covalently linked to the surface of the droplets and bright fluorescence from the BODIPY dye was observed at the hydrocarbon-water interface as shown in **Figure 3.1.** In the control experiments under the same conditions without GA16-MA in the droplet phase, no fluorescent ring was observed by confocal microscopy (shown in supporting information **Figure 3.5**).

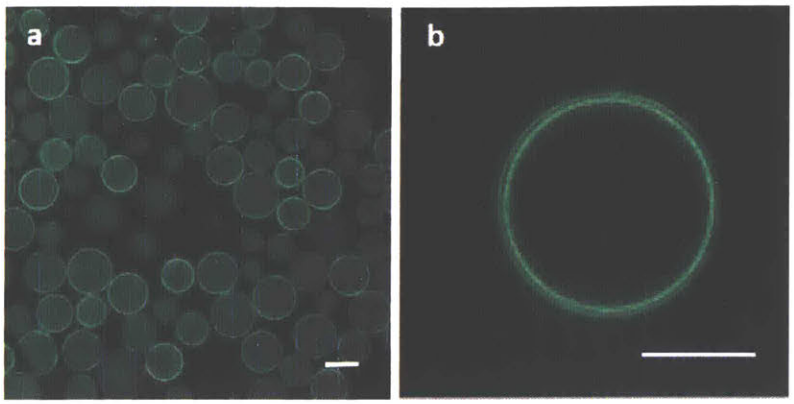

Figure 3.1. Confocal microscopy images of cysteine-BODIPY functionalized droplets using interfacial maleimide-thiol chemistry. Scale bar in 50 μm. a) Confocal z-stack images of emulsion droplets containing GA16-MA after covalent dye functionalization, 10 X magnification. b) Confocal cross-section of the droplet containing GA16-MA after covalent dye functionalization, 20 X magnification.

3.3.4 Controlled conjugation reactivity of the emulsion assays

Our complex emulsion assays rely exclusively on the interfacial functionalization and the recognition characteristics thereof. The droplet interface is dynamic and the morphology switches between H/F/W, Janus, and F/H/W with changes in the interfacial tensions between hydrocarbon-water interface and fluorocarbon-water interface.[14] Another advantage of the emulsion droplets is that they can provide hydrolytic stability for the reactants that are localized in an internal phase that initially doesn't share an interface with water. With controlled activation the reactant can be used for functionalization at later times.

As shown in **Scheme 3.4**, GA16-MA and BODIPY-FL-Cysteine was used to demonstrate the controlled interfacial conjugation. Tween 20 was chosen as the continuous phase "activating" hydrocarbon surfactant. Together with Zonyl as the continuous phase fluorocarbon surfactant, it is possible to tune the morphology of the droplets to facilitate maleimide-thiol conjugation. Tween

20 was chosen because of its mild surfactant behavior, which means it will not completely cover the hydrocarbon-water interface but is still able to change the morphology of the droplets. In the H/F/W morphology state, wherein the hydrocarbon oil was encapsulated inside the fluorocarbon phase, GA16-MA is rendered inert. When the droplet morphology was switched to Janus or F/H/W by the addition of Tween 20, the hydrocarbon phase now has a reactive interface with water and the interfaces are activated for functionalization reactions.

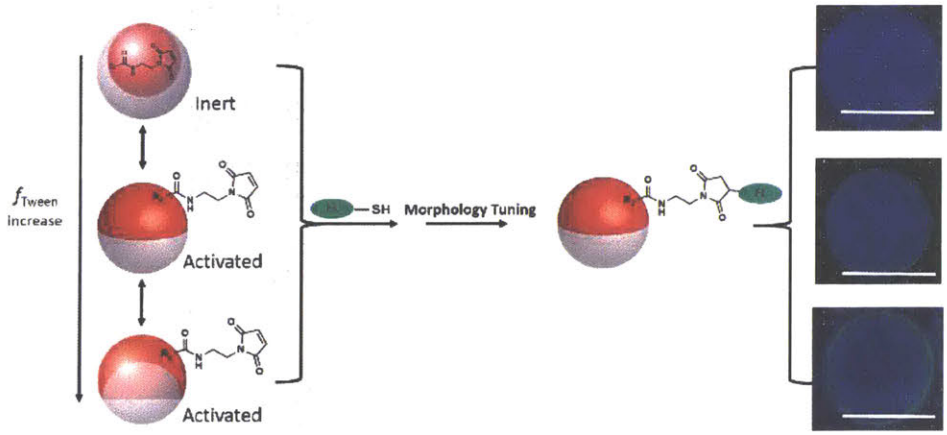

Scheme 3.4. Dynamic emulsion droplets with controlled reactivity. Droplets start in different morphology and functionalized at the hydrocarbon-water interface. Droplets were then tuned to the Janus morphology for imaging. Higher intensity in green channel indicates higher level of functionalization at the interface. Higher intensity in green channel indicates higher functionalization at interface.

3.3.5 Quantification of the interfacial conjugation reaction

To further quantify the level of covalent functionalization at the interface, anthracene with different emission wavelength from BODIPY was used as an internal fluorescent reference to indicate the amount of fluorophore functionalized at the droplet interface. As shown in **Scheme 3.4**, the droplets with different starting morphology were functionalized with BODIPY using maleimide-thiol chemistry. After the reaction, the morphology of the droplets was tuned to the exact Janus state for confocal imaging by changing the continuous phase surfactant with either Zonyl or Tween 20. The fluorescent intensity of both fluorophores are analyzed through the open

access software ImageJ (National Institute of Health, Bethesda, MD, USA; available for download at https://imagej.nih.gov/ij/) and the relative intensity ratio between $E_{anthracene}$ and E_{BODIPY} was plotted against the initial droplet morphology, indicated by relative surfactant ratio f_{Tween} (**Figure 3.2**). The more surface area at the hydrocarbon-water interface during conjugation, the more thiol is functionalized as indicated by the BODIPY fluorescent intensity.

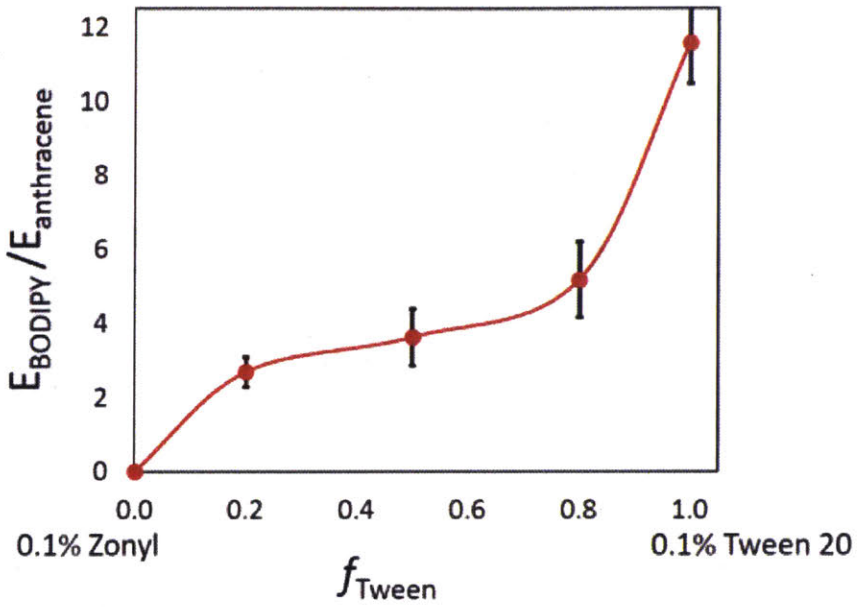

Figure 3.2. The ratio of emission intensity at the interface (E_{BODIPY}) and inside ($E_{anthracene}$) relative to the continuous tween 20 surfactant concentration. The higher concentration of tween, the more surface area for the hydrocarbon-water interface.

3.4 Biomolecule functionalized emulsion assays

3.4.1 Protein A functionalized assay for IgG detection

We have shown that the emulsion droplets containing GA based reactive surfactants can be functionalized with molecules bearing free amine or thiol group. Functionalization with biomolecules is necessary to achieve broad utility in biosensing assays. As a proof-of-concept, we have targeted a Protein A functionalized emulsion assay for the binding of anti-mouse IgG. As

shown in **Scheme 3.5**, Protein A reacts through amines with Janus emulsion droplets containing GA12-NHS.

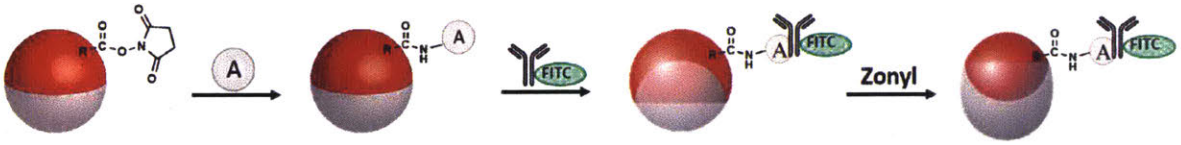

Scheme 3.5. Droplet functionalization with protein A and detection scheme with immunoglobulin (IgG).

After functionalization, the emulsion droplets maintained a Janus morphology (**Figure 3.3a**). Addition of FITC (fluorescein isothiocyanate) labelled anti-mouse IgG to the continuous phase results in binding to Protein A on the surface of droplets. This modification resulted in a change in droplet morphology from Janus to a F/H/W double emulsion (**Figure 3.3b**). The binding of IgG to the droplet surface was further validated with confocal microscopy. The bright green fluorescence from the FITC labeled IgG was observed under confocal microscopy and was only located at the hydrocarbon-water interface (**Figure 3.3c**). We rationalize that the large IgG molecule provides additional hydrophilic character, which increases the surfactant strength at the hydrocarbon-water interface, thereby expanding the organic water interface. The GA12-NHS is

therefore established as an active biomolecular reactive group for functionalization of the hydrocarbon-water interface.

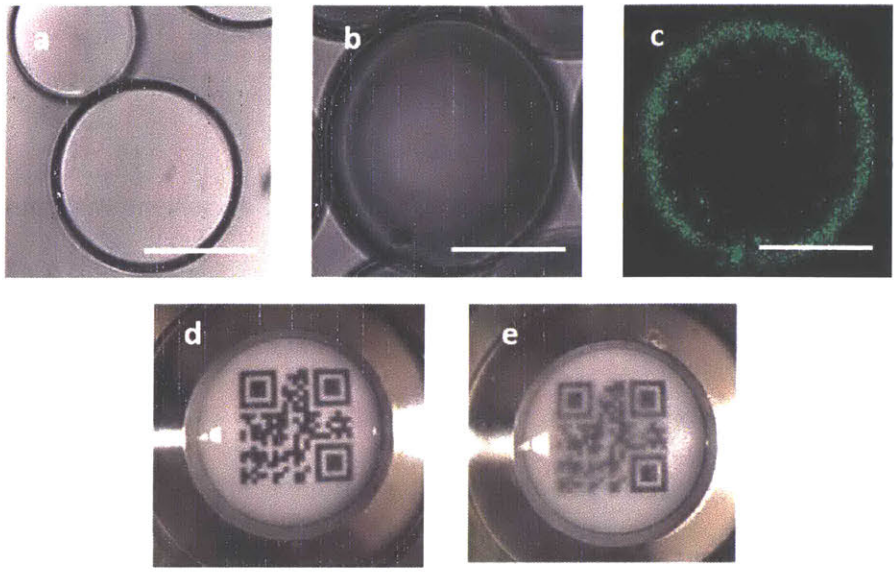

Figure 3.3. Protein A functionalized emulsion droplet for the detection of anti-mouse IgG. Scale bar in 50 μm. a) Microscope image of Protein A functionalized droplets in Janus morphology. b) Microscope image of droplet in F/H/W after IgG bind to protein A. c) Confocal cross section image of droplets with IgG at the hydrocarbon-water interface, in F/H/W morphology. d) Protein A functionalized transparent Janus droplets enables scanning of the QR code. e) After IgG binding to protein A, F/H/W emulsions droplets become less transparent and blocks the QR code information.

This morphology change from Janus (transparent) to F/H/W (opaque) is easily visualized with the transmission of natural light through thin gravity aligned layers of emulsion droplets without fluorescent labelling.[12,14] We have shown the change qualitatively using the QR code method before (**Figure 3.3d**) and after (**Figure 3.3e**) binding of IgG to the protein A functionalized emulsions assay. This morphology change is different from the agglutination scheme reported in our previous study,[12] in a way that all the droplets have changed from Janus to F/H/W instead of forming aggregates. The macroscopic change can still be visualized using the QR code method but not quantitatively with the graphical counting method. Another optical method to quantify the morphology change will be reported in a follow-up study.

To demonstrate there is covalent bond between the droplet and Protein A/IgG complex, additional Zonyl surfactant was added in the continuous phase to force a morphology change from F/H/W to H/F/W. The Protein A/IgG complex is not dislodged from the hydrocarbon-water interface and the added Zonyl produces a deformation (**Figure 3.4**) from a perfect sphere. If the droplet was not functionalized with proteins, the hydrocarbon phase would become an inner phase of a double emulsion, H/F/W. This experiment also shows that the interface was still dynamic after functionalization of either Protein A or IgG. Preserving a dynamic interface is central to sensing opportunities and producing changes in droplet morphology.[11]

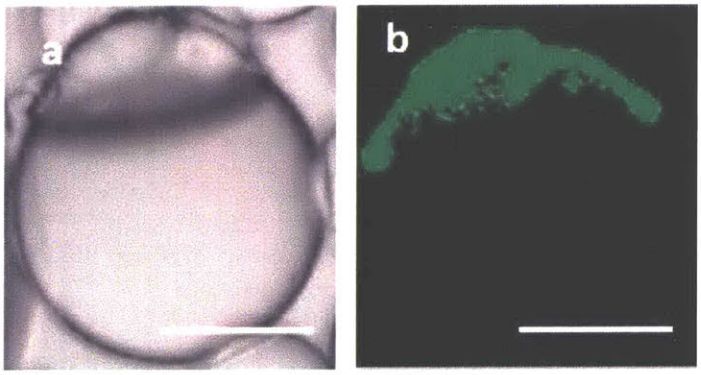

Figure 3.4. Images of Zonyl forced droplets after IgG binding to protein A. Scale bar in 50 μm. a) Zonyl forced deformation of emulsion droplet on the side under microscope. b) Confocal z-stack images of deformed droplets showing covalent bond formation at the droplet interface.

3.4.2 Nucleic acid and carbohydrate functionalization

To demonstrate the generic bioconjugation capabilities of the emulsion assay, broader types of biomolecules were functionalized to the droplets (**Scheme 3.6**). Confocal Images of the functionalized droplets were shown in **Figure 3.7**.

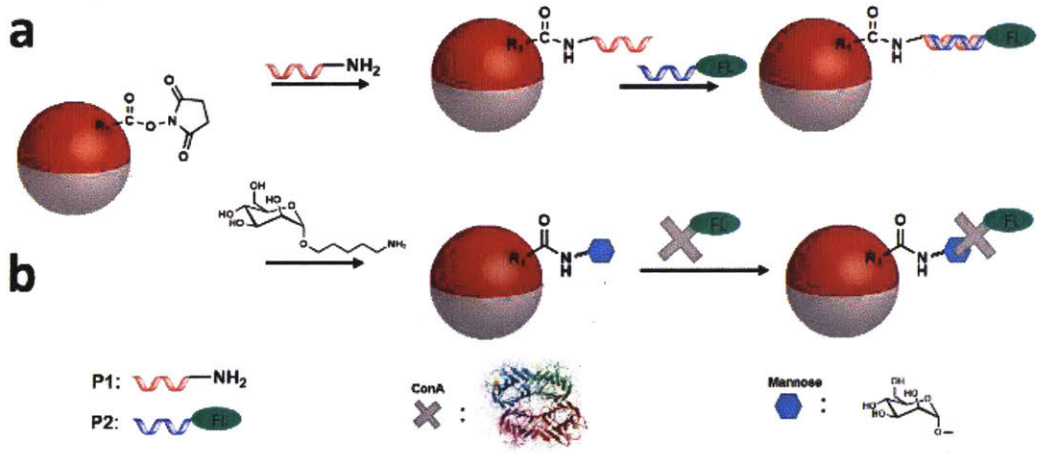

Scheme 3.6. a) Bioconjugation with oligonucleotide followed by hybridization. b) Bioconjugation with mannose derivative for the binding of concanavalin A.

A strand of oligonucleotide 5'-amine C6 linker modified P1 was covalently functionalized to the droplet surface with GA12-NHS and amine reaction. A complementary strand P2 bearing a (6-carboxyfluorescein) 6-FAM tag at the 5' was added in the continuous phase. After removing unreacted oligonucleotide by washing, fluorescence from FAM was observed under confocal microscopy at the hydrocarbon-water interface, which indicates the oligonucleotide still maintains the reactivity.

A mannose bearing amine was functionalized to the droplets using NHS-amine chemistry. Concanavalin A (ConA) labelled with FITC was added in the continuous phase. After washing the excess ConA from the mixture, fluorescence from FITC was observed under confocal microscopy, showing the carbohydrate-lectin binding interactions were preserved.

3.5 Conclusion

We have designed an emulsion assay capable of bioconjugation using NHS-amine or maleimide-thiol chemistry. This assay has provided a generic platform for functionalization of biomolecules to the emulsion droplets as biosensors with antibodies, enzymes, nucleic acids and carbohydrates. The dynamic interface and droplet morphologies enable the controlled interfacial reactivity. The detection of IgG with protein A functionalized droplet assay was demonstrated using morphological changes that are easily detected with natural light transmission. Quantitative optical method and sensing of other targeted biomolecule will be demonstrated in follow-up studies.

3.6. Experimental Section

3.6.1. General methods and instrumentation

Diethylbenzene (DEB), 2-(trifluoromethyl)-3-ethoxydodecafluorohexane (HFE 7500), hydroxylamine, trifluoroethanol, phosphate-buffered saline (PBS, pH = 7.6) (1 M), Tris buffer (pH = 8.0), HEPES buffer (pH = 7.6), Zonyl FS-300, fluoresceinamine, tris(2-carboxyethyl)phosphine hydrochloride (TCEP), N-(3-Dimethylaminopropyl)-N'-ethylcarbodiimide hydrochloride (EDC), N-hydroxysuccinimide (NHS), Concanavalin A-FITC, anti-mouse IgG-FITC and Protein A were purchased from Sigma-Aldrich. BODIPY FL L-Cysteine was purchased from ThermoFisher. Sulfo-Cyanine3 amine was purchased from Lumiprobe. Solvents were purchased from Sigma-Aldrich and used as received. Oligonucleotides were purchased from Integrated DNA Technologies (IDT) and used without further purification.

EDC and NHS were dissolved in PBS at 1 M and prepared fresh before each usage. Continuous phase surfactants were prepared as stock solution in PBS, including 0.1 wt% and 0.01

wt% Zonyl FS-300 as the fluorocarbon surfactant and 0.1 wt% Tween 20 as the hydrocarbon surfactant. Hydroxylamine was prepared as 1M solution in PBS to quench unreacted NHS groups at the droplet interface.

NMR spectra were recorded using a Bruker Avance 400 MHz NMR spectrometer and were referenced to the proton resonances resulting from incomplete deuteration of NMR solvent (^{1}H). Confocal microscopy images were taken at room temperature with Nikon A1R Ultra-Fast Spectral Scanning Confocal Microscope.

3.6.2. Emulsion Assay Preparation

3.6.2.1. Bulk emulsification for polydispersed complex emulsion droplets

Complex emulsions, composed of equal volumes of diethylbenzene and HFE 7500 in aqueous continuous phase were fabricated using bulk emulsification, which generates polydisperse droplets (20-100 μm in diameter). In this process, the hydrocarbon phase (DEB) and fluorocarbon phase (HFE 7500) were mixed and heated above the upper critical temperature (around 40 °C) to generate a single droplet phase. This single droplet phase was then dispersed into the aqueous phase containing the continuous phase surfactants to generate single phase emulsions and upon cooling to room temperature, the DEB and HFE 7500 phases separated to generate complex emulsions. The composition of all droplets was identical because every droplet originated from the same single phase.[11]

A generic assay contains 0.5 mL of continuous phase and 20 μL droplet phase.

3.6.2.2. GA12OH assay preparation

To generate emulsion droplets containing GA12OH for interfacial functionalization, GA12OH was dissolved with gentle heat at 10 mg/mL in DEB. Polydispersed complex emulsion droplets were fabricated via bulk emulsification described above with 0.01 wt% Zonyl as the continuous phase surfactant. 25 μL of EDC solution was added to the emulsion and reacted for 15 min followed by addition of 25 μL of NHS solution. The reaction was set at room temperature for 1 h on a rocker (Rocker II from Boekel Scientific). The resulting assay is in equivalent to a GA12-NHS assay.

3.6.2.3. GA12-NHS assay preparation and fluoresceinamine functionalization

GA12-NHS was dissolved at 10 mg/mL in DEB. Trifluoroethanol was added at 10% in volume to the hydrocarbon and fluorocarbon mixture to decrease the mixing temperature. A mixture of 0.1 wt% Zonyl : 0.1 wt% Tween 1:1 (v/v) was used as the continuous phase to increase the hydrocarbon-water surface area for bioconjugation. After emulsification, the continuous phase was exchanged twice with the same mixture of 0.1 wt% Zonyl : 0.1 wt% Tween 1:1 (v/v) to remove the trifluoroethanol from the emulsion assay.

Fluoresceinamine was prepared as 0.5 mg/mL solution in PBS. 25 μL of the fluoresceinamine solution was added to the GA12-NHS assay and reacted at room temperature overnight on a rocker. The continuous phase was washed 5 times after reaction to remove the excess amount of dye before imaging.

Sulfo-Cyanine 3 amine was prepared as 1mg/mL solution in PBS. 25 μL of the Sulfo-Cyanine 3 amine solution was added to the GA12-NHS assay. The reaction was carried out overnight at room temperature. Two vials containing different dye functionalized droplets were combined together. The mixture was settled for 48 h before imaging.

3.6.2.4. GA16-MA assay preparation and BODIPY-FL-Cysteine functionalization

GA16-MA was dissolved at 10 mg/mL in DEB and the assay was prepared using the same method as described for the GA12-NHS assay.

BODIPY-FL-Cysteine was first dissolved in PBS at 1 mg/mL and activated with TCEP. The activated dye solution become bright green within 15 min and 25 μL of the activated dye solution was added to the GA16-MA assay. The continuous phase was washed 5 times after overnight reaction to remove excess amount of dye before imaging.

3.6.2.5 Protein A functionalization and IgG detection

Protein A was dissolved at 0.5 mg/mL in PBS buffer. 25 μL of the Protein A solution was added to a GA12-NHS assay and reacted overnight at room temperature on a rocker. The reaction was stopped with 25 μL of hydroxylamine solution to quench any unreacted NHS groups at the droplet surface. The continuous phase was washed with surfactant solution for three times. 25 μL anti-mouse IgG with FITC label from Sigma-Aldrich was added to the Protein A functionalized assay and reacted for 2 h. The continuous phase was then washed with surfactant solution for five times to remove unreacted IgG before imaging. For the QR code detection method, the emulsion solution before and after IgG addition was images in a stainless steel chamber with a glass bottom. The droplets naturally sit at the bottom of the chamber due to gravity and cover the glass bottom. The QR code was printed on a piece of paper and placed under the chamber.

3.6.2.6 Oligonucleotide functionalization

GA12-NHS assay was prepared as described in the previous section. 3 μL of oligonucleotide P1 with a sequence of 5'-NH_2-$(CH_2)_6$-TTT TTT TTT T AGA GTT GAG CAT-3' at 2 mM in PBS solution was added in the continuous phase. The conjugation reaction was carried

out overnight at room temperature. The reaction was quenched with addition of 100 μL of 1 M Tris buffer solution. 3 μL of complementary strand of oligonucleotide P2 with a sequence of FAM-5'-TTT TTT TTT T ATG CTC AAC TCT-3' at 1 mM in PBS solution was added. The solution was heated up to 50 °C and held for 15 min using a water bath. The emulsion assay was then allowed to cool down to room temperature and the continuous phase was washed 5 times to remove the unreacted oligonucleotide. During the annealing process, the hydrocarbon and fluorocarbon phase will become miscible and form one droplet phase once heated above the upper critical temperature, but the mixture will phase separate and form complex emulsions again after cooling down.[11]

3.6.2.7 Carbohydrate functionalization

GA12-NHS assay was prepared as described in the previous section. Man-C5-NH_2 was dissolved in PBS at 1 mg/ml. 50 μL of Man-5-NH_2 solution was added in the continuous phase and reacted overnight at room temperature. The reaction was quenched with 100 μL of 1 M Tris buffer solution. 10 μL of 1 mg/mL FITC labelled Con A in HEPES buffer was added and reacted for 30 min. The solution was then washed 5 times to remove the excess lectin before imaging.

3.6.2.8 Droplet morphology Tuning

The droplets morphology can be tuned by using different compositions of the hydrocarbon/fluorocarbon surfactant mixture. After bioconjugation of the droplets shown in previous sections, addition of hydrocarbon/fluorocarbon surfactant could further change the morphology of the droplets because the droplets interface maintain dynamic. Droplets are in the perfect Janus state when there is a single circle to be focused under microscope (**Figure 3.3a**).

3.6.3. Synthetic Procedures

3.6.1. Synthesis of GA12OH

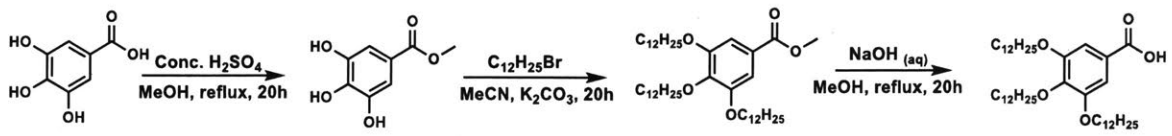

Scheme 3.7 Synthesis of GA120H.

GA12OH was synthesized according to a modification of a published procedure.[16]

^{1}H NMR (400 MHz, $CDCl_3$): δ 7.32 (s, 2H), 4.06-4.01 (m, 6H), 1.84-1.73 (m, 6H), 1.51-1.44 (m, 6H), 1.35-1.27 (m, 48H), 0.89-0.86 (m, 9H)

3.6.2. Synthesis of GA12-NHS

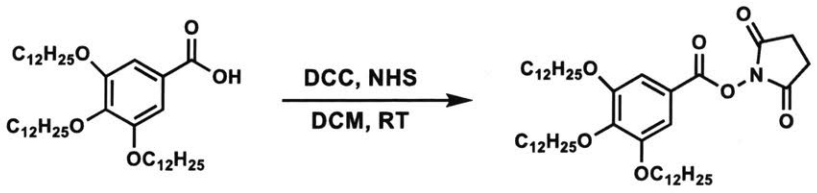

Scheme 3.8 Synthesis of GA12-NHS.

GA12-NHS was synthesized according to a modification of a published method.[17] GA12OH (1 g, 1.3 mmol), N,N'-dicyclohexylcarbodiimide (0.347 g, 1.7 mmol) and N-hydroxysuccinimide (0.194 g, 1.7 mmol) were dissolved in 50 mL dichloromethane followed by addition of catalytic amount of DMF. The solution was stirred at room temperature overnight. The crude material was purified by silica gel column chromatography using hexane and EtOAc (4/1).

^{1}H NMR (400 MHz, $CDCl_3$): δ 7.32 (s, 2H), 4.07-3.99 (m, 6H), 2.92-2.89 (m, 4H), 1.85-1.78 (m, 4H), 1.75-1.70 (m, 2H), 1.50-1.43 (m, 6H), 1.36-1.26 (m, 48H), 0.89-0.86 (m, 9H)

3.6.3 Synthesis of GA16-MA

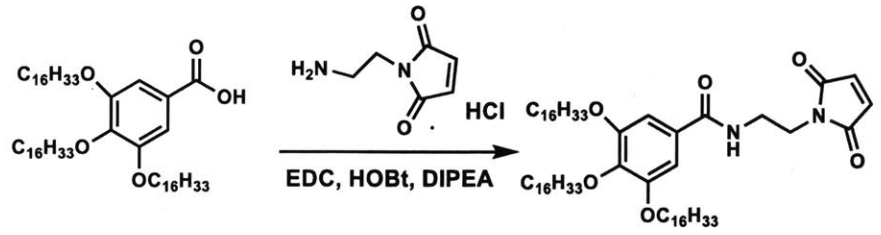

Scheme 3.9 Synthesis of GA16-MA

GA16OH was used for the synthesis of GA16-MA to increase the solubility in hydrocarbon. To a solution of GA16OH (0.5 g, 0.60 mmol) in dichloromethane (10 mL) was added N,N-diisopropylethylamine (0.85 ml, 6 mmol). The mixture was treated with N-(3-dimethylaminopropyl)-N'-ethylcarbodiimide hydrochloride (0.19 g, 1 mmol), 1-hydroxybenzotriazole (0.13 g, 1 mmol) and N-(2-aminoethyl)maleimide hydrochloride (0.116 g, 0.66 mmol) and stirred at room temperature overnight. The reaction was quenched with droplet of HCl (1 M) solution and washed with water for three times. The organic portion was dried over Na_2SO_4. The crude material was purified by silica gel column chromatography using hexane and EtOAc (4/1 to 3/1).

^{1}H NMR (400 MHz, $CDCl_3$): δ 6.96 (s, 2H), 6.73 (s, 2H), 6.58 (t, J=4.6 Hz, 1H), 4.04-3.96 (m, 6H), 3.84-3.82 (m, 2H), 3.66-3.62 (m, 2H), 1.83-1.71 (m, 6H), 1.49-1.45 (m, 6H), 1.37-1.26 (m, 72H), 0.90-0.86 (m, 9H). ^{13}C NMR (400 MHz, $CDCl_3$): δ171.05, 167.48, 153.06, 134.30, 128.88, 105.43, 73.47, 69.20, 39.99, 37.44, 31.94, 30.33, 29.76-29.67, 29.60, 29.38, 26.10, 22.70, 14.13. HRMS (ESI): Calculated for $C_{61}H_{108}N_2O_6$ ($[M+H]^+$): 965.8286 , found 965.8264. ATR-IR (Ge, cm^{-1}): 2918 (C-H), 2849 (C-H), 1697 (C=O).

3.6.4. Confocal Images

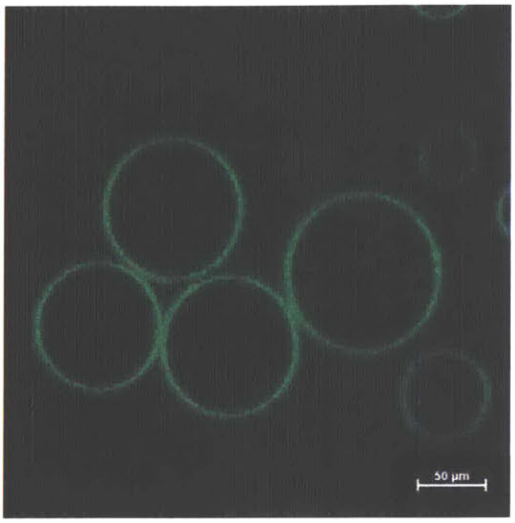

Figure 3.5. Confocal image of droplet functionalized with fluoresceineamine using Scheme 3.3a/b.

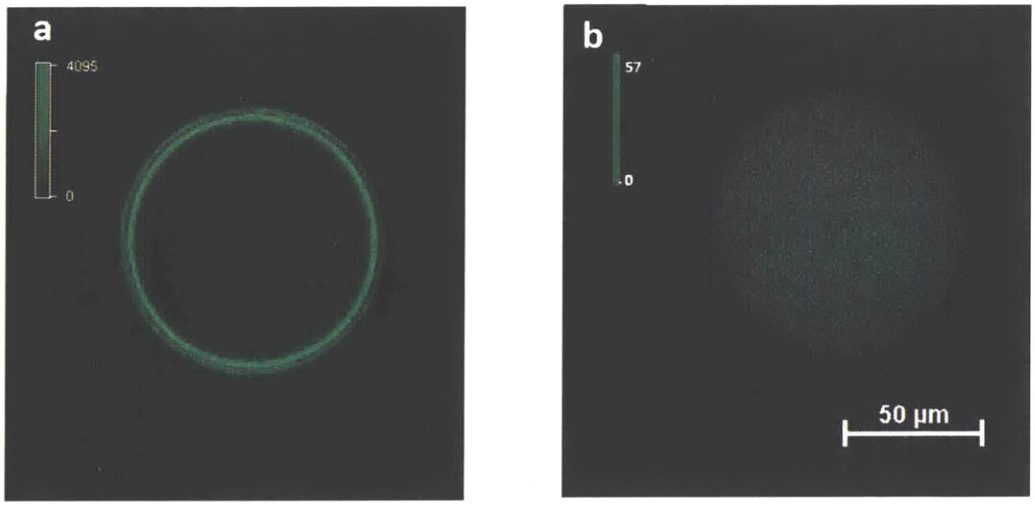

Figure 3.6. a) Confocal image of BODIPY-FL-Cysteine treating droplets with GA16-MA loaded in the droplets. Color bar showing the fluorescent intensity. b) Pristine droplet treated with the same concentration of BODIPY-FL-Cysteine and no bright ring was observed. Light fluorescence inside the droplet indicates minor solubility of the fluorophore in the droplet phase.

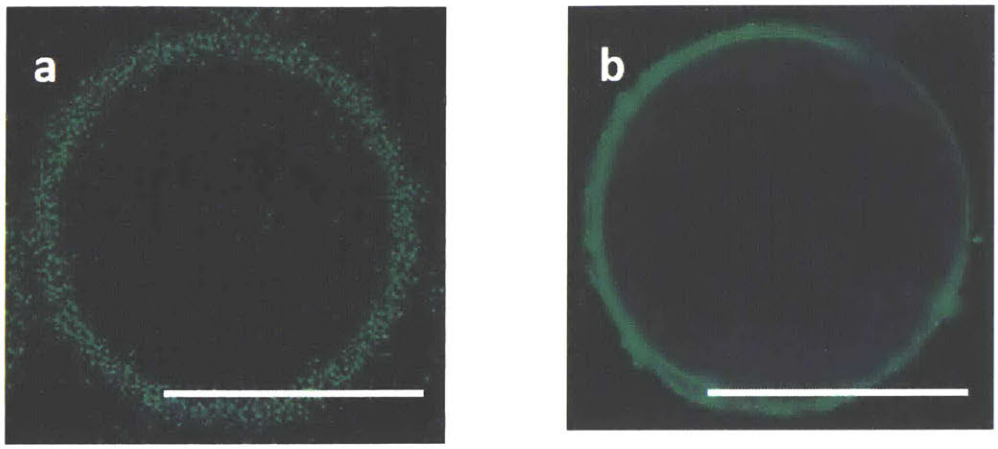

Figure 3.7 a) Confocal image of oligonucleotide P1 functionalized droplet with complementary strand P2 bearing a 6-FAM fluorophore (**Scheme 3.5a**). b) Confocal image of mannose functionalized droplet binds to ConA-FITC (**Scheme 3.5b**). Scale bar in 50 μm.

3.7 References

(1) Turner, A. P. F.; Karube, I.; Wilson, G. S. Biosensors : *Fundamentals and Applications.* Oxford University Press; **1987**.

(2) Banica, F.-G. *Chemical Sensors and Biosensors : Fundamentals and Applications*; John Wiley & Sons Inc, **2012**.

(3) Amine, A.; Mohammadi, H.; Bourais, I.; Palleschi, G. Enzyme Inhibition-Based Biosensors for Food Safety and Environmental Monitoring. *Biosens. Bioelectron.* **2006**, 21 (8), 1405–1423.

(4) Edmondson, R.; Broglie, J. J.; Adcock, A. F.; Yang, L. Three-Dimensional Cell Culture Systems and Their Applications in Drug Discovery and Cell-Based Biosensors. *Assay Drug Dev. Technol.* **2014**, 12 (4), 207–218.

(5) Luppa, P. B.; Sokoll, L. J.; Chan, D. W. Immunosensors. *Principles and Applications to Clinical Chemistry. Clin. Chim. Acta* **2001**, 314 (1–2), 1–26.

(6) Junhui, Z.; Hong, C.; Ruifu, Y. DNA Based Biosensors. *Biotechnol. Adv.* **1997**, 15 (1), 43–58.

(7) Wang, J. Electrochemical Glucose Biosensors. *Chem. Rev.* **2008**, 108, 814–825.

(8) Wang, J. Carbon-Nanotube Based Electrochemical Biosensors: A Review. *Electroanalysis* **2005**, 17 (1), 7–14.

(9) Tombelli, S.; Minunni, M.; Santucci, A.; Spiriti, M. M.; Mascini, M. A DNA-Based Piezoelectric Biosensor: Strategies for Coupling Nucleic Acids to Piezoelectric Devices. *Talanta.* **2006**, 68 (3), 806–812.

(10) Chen, P.; He, C. A General Strategy to Convert the MerR Family Proteins into Highly Sensitive and Selective Fluorescent Biosensors for Metal Ions. *J. Am. Chem. Soc.* **2004**, 126 (3), 728–729.

(11) Zarzar, L. D.; Sresht, V.; Sletten, E. M.; Kalow, J. a.; Blankschtein, D.; Swager, T. M. Dynamically Reconfigurable Complex Emulsions via Tunable Interfacial Tensions. *Nature* **2015**, 518 (7540), 520–524.

(12) Zhang, Q.; Savagatrup, S.; Kaplonek, P.; Seeberger, P. H.; Swager, T. M. Janus Emulsions for the Detection of Bacteria. *ACS Cent. Sci.* **2017**, 3 (4), 309–313.

(13) Nagelberg, S.; Zarzar, L. D.; Nicolas, N.; Subramanian, K.; Kalow, J. A.; Sresht, V.; Blankschtein, D.; Barbastathis, G.; Kreysing, M.; Swager, T. M.; Kolle, M. Reconfigurable and Responsive Droplet-Based Compound Micro-Lenses. *Nat. Commun.* **2017**, 8, 14673.

(14) Zarzar, L. D.; Kalow, J. A.; He, X.; Walish, J. J.; Swager, T. M. Optical Visualization and Quantification of Enzyme Activity Using Dynamic Droplet Lenses. *Proc. Natl. Acad. Sci.* **2017**, 114 (15), 201618807.

(15) Shi, C.; Zhang, L.; Xie, L.; Lu, X.; Liu, Q.; Mantilla, C. A.; Van Den Berg, F. G. A.; Zeng, H. Interaction Mechanism of Oil-in-Water Emulsions with Asphaltenes Determined Using Droplet Probe AFM. *Langmuir.* **2016**, 32 (10), 2302–2310.

(16) Achalkumar, A. S.; Hiremath, U. S.; Rao, D. S. S.; Prasad, S. K.; Yelamaggad, C. V. Self-Assembly of Hekates-Tris(N -Salicylideneaniline)s into Columnar Structures: Synthesis and Characterization. *J. Org. Chem.* **2013**, 78 (2), 527.

(17) Corbin, P. S.; Zimmerman, S. C.; Thiessen, P. A.; Hawryluk, N. A.; Murray, T. Complexation-Induced Unfolding of Heterocyclic Ureas. Simple Foldamers Equilibrate with Multiply Hydrogen-Bonded Sheetlike Structures. *J. Am. Chem. Soc.* **2001**, 123, 10475-10488.

CHAPTER 4

Emulsion Agglutination Assay for Sensing of Zika Virus

The work presented in this chapter is a manuscript in preparation for submission. This chapter represents a collaboration between the author and Dr. Lukas Zeininger, who designed and conducted the inner filter effect measurements. The author thank Kosuke Yoshinaga for providing the fluorous dye F-PDI. The author thank Ki-Joo Sung and Eric Miller from Prof. Hadley D. Sikes group in Department of Chemical Engineering at MIT for the synthesis of Sso7d proteins and helpful discussions.

4.1 Introduction

Zika virus (ZIKV) is a type of flavivirus that is spread mostly by mosquitoes. The infection of the Zika virus causes mild symptoms to adults but can be passed from pregnant women to her fetus and causes severe birth defects. There is no effective vaccines or medicines for Zika currently, so the detection of Zika virus would be essential to lower the risk for newborn defect. Many researchers have spent the effort to develop assays for the detection of Zika virus including polymerase chain reaction (PCR)[1] and antibody based (ELISA)[2] assays. Additionally, detection of Zika virus using RNA amplification and CRISPR method for the rapid and low-cost sensors has been reported to be used in pandemic regions.[3] However, a sensing assay with high stability and minimum amount of handling effort has not been reported and will become essential in the area with high risk of Zika infection.

Our group has reported a new class of complex smart colloids[4] and have demonstrated the ability of sensing assays for antibodies[5] and bacteria[6]. The advantage of such smart colloids are their intrinsic optical properties[7] and the ability of interfacial bioconjugation for targeted binding behavior. Herein, we report an expanded agglutination assay for the detection of Zika virus non-structural proteins NS1, which has multiple roles in pathogenesis and immune evasion.[8]

The key to the sensitivity in this emulsion assay is the binding of surfactant molecule to the analyte, and the translation of the binding into agglutination, which is then detected via change of optical transmission of the emulsion droplets. To anchor recognition elements to complex colloids, we use the surfactants based upon maleimide functionalized polystyrene-polyacrylic acid P1-MA for the binding of a thiol group on a thermally stable protein, which binds the target Zika NS1 protein. The thermally stable protein is used as a substitute of an antibody to produce sensors that can survive in extreme conditions including high temperature. The protein recognition

elements were also chosen because they can be produced in large quantity and exhibit good binding strength to the target protein.[9] We designed an agglutination assay using the thermal stable protein Sso7d that binds to streptavidin in order to optimize the system. An optical system was developed using inner filter effect of two dyes in both the hydrocarbon and fluorocarbon phases for the transduction of the biological binding to an electronic signal. The optimized system was applied for the detection of Zika NS1 protein and we are able to achieve a detection limit of 0.1 μM. Our emulsion assay's sensitivity is in the same level of the literature reported NS1 detection limit, and with the advantage of thermal stable and minimum usage of complex equipment, oligonucleotide extraction and requirement of trained technician.

4.2 Results and Discussion

Previously, we have reported a gallic acid derivative as the surfactant for bioconjugation as detailed in Chapter 3. Although the gallic acid molecules exhibits good stability at the droplet interface for bioconjugation and resulted morphology changes as the sensing mechanism, we found that small molecule are not strong enough anchors to hold multiple droplets together for a protein-protein agglutination assay. We therefore have moved to polymeric anchors and have used a polystyrene-polyacrylic acid based surfactant P1 to increase the connection between the protein and droplets. The acrylic acid block on polymer P1 was functionalized with maleimide-NH_2 to form P1-MA (**Scheme 4.1a**). P1-MA was dissolved in the hydrocarbon phase as a hydrocarbon/water (H/W) interfacial active agent and the maleimide group exposed in the aqueous phase can be bioconjugated with cysteine engineered proteins to form protein specific droplet assays.

For protein-protein interaction, we used a hyperthermophilic protein as the antibody alternative to specifically capture targeted analyte proteins. This class of thermally stable proteins,

named Sso7d, was produced using a combination of rational design and directed evolution to convert a native DNA binding protein into protein specific binders.[9] In this study, a streptavidin specific Sso7d was produced and a cysteine residue was engineered to the N-terminus for bioconjugation to droplets. Sso7d was covalently linked to the hydrocarbon-water (H/W) interface via maleimide-thiol chemistry. The addition of streptavidin to the Sso7d functionalized droplet assay causes the droplets to agglutinate because streptavidin is a tetramer, and could link the Sso7ds from different droplets together to form aggregates (**Scheme 4.1b**).

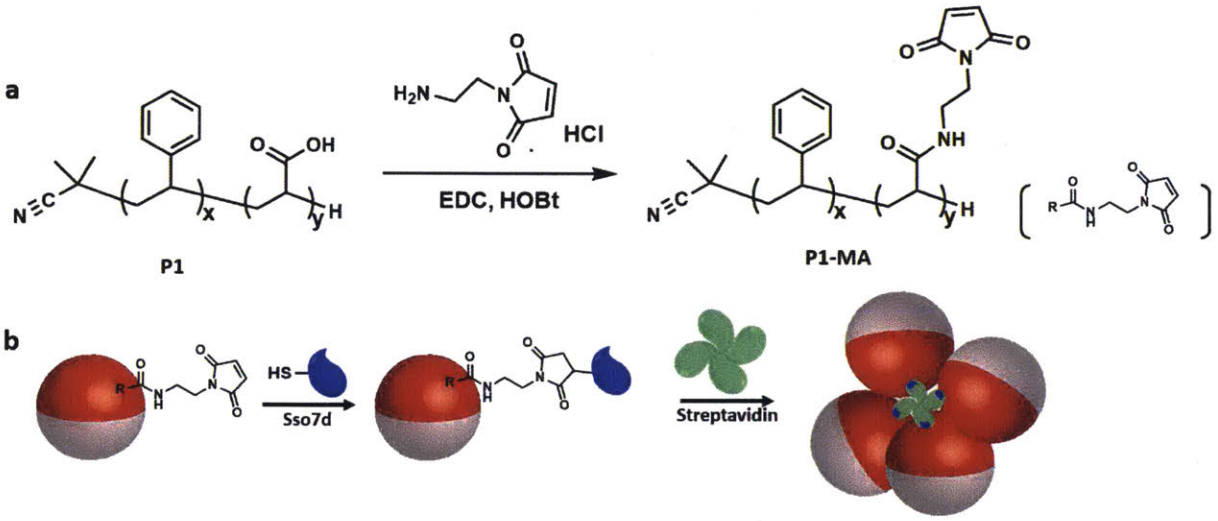

Scheme 4.1. a.) Synthesis of maleimide functionalized surfactant P1-MA from a polystyrene-polyacrylic acid polymer. b.) Bioconjugation of Sso7d to the droplet H/W interface via maleimide-thiol chemistry. The addition of streptavidin to the Sso7d functionalized droplets assay cause agglutination. The hydrocarbon phase is shown in red for display purpose. Scheme not to scale.

The amount of Sso7d that was functionalized to the droplet H/W interface is different based on the initial droplet morphology. To optimize the level of functionalization of Sso7d for agglutination, three initial morphologies at H/F/W, Janus and F/H/W were tested by tuning the composition of the continuous phase (H_2O) surfactant. As shown in **Scheme 4.2**, droplets start in different morphologies, and after Sso7d functionalization, droplets in the three tests were switched to Janus state before adding streptavidin for comparison of the level of agglutination. The

micrographs in **Scheme 4.2** reveal that droplets starting in the F/H/W morphology give the most effective agglutination. These results indicate that higher surface area at the H/W interface facilitates the functionalization with Sso7ds, and increases the agglutination sensitivity. Tween 20, also a hydrocarbon surfactant, at higher concentration in the assay could potentially compete at the H/W interface with P1-MA, but the P1-MA molecule appears to exhibits stronger surfactant behavior, which indicated that Tween 20 did not fully cover the H/W interface in the F/H/W morphology and block the interfacial maleimide-thiol reaction. As a result, the Sso7d functionalization step in the following studies are all carried out at F/H/W morphology.

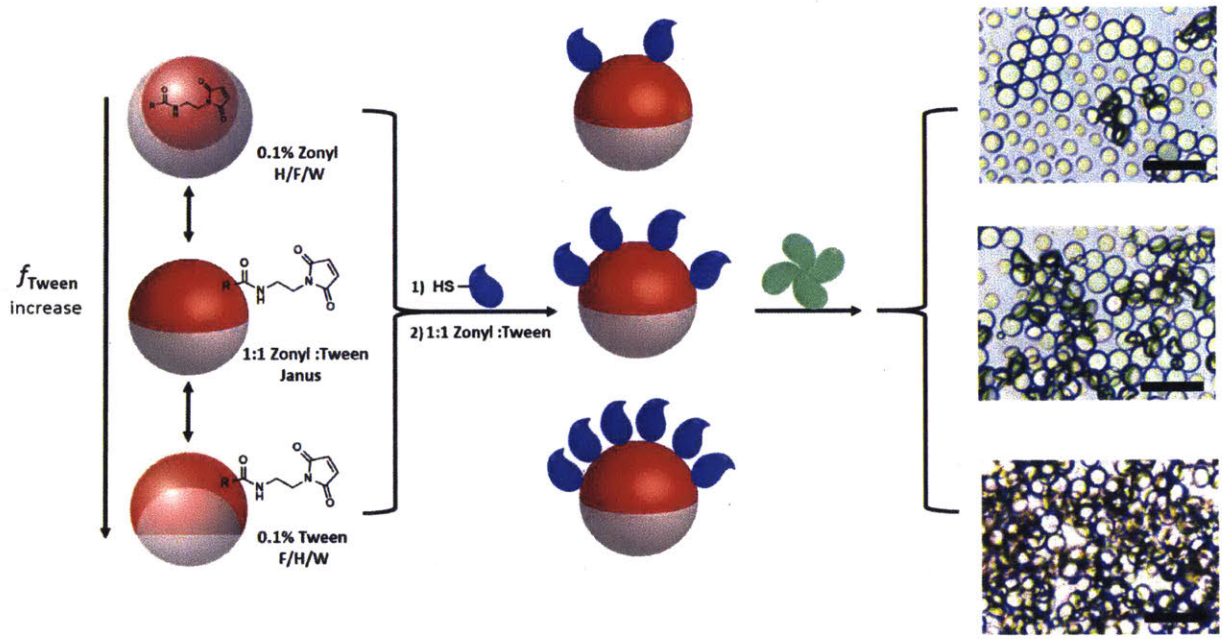

Scheme 4.2. Droplets starting at different morphologies, namely H/F/W, Janus and F/H/W functionalized with cysteine engineered Sso7d. The continuous phase was exchanged to tune the morphology into Janus followed by addition of 10 μL of 1mg mL^{-1} streptavidin. The micrographs were taken with optical microscope at 10 x magnification. Scale bar equals 100 μm.

We have previously reported the intrinsic optical properties of the droplets as lenses,[7] and how different morphologies are readily detected by their light transmission/scattering characteristics.[10] To further magnify the optical differences between the naturally gravity oriented

and tilted droplets, we employ a new design using the inner filter effect (IFE) for the agglutination assay in this study. Two fluorophores were separately added to the hydrocarbon and fluorocarbon phase, namely perylene, and F-PDI (**Figure 4.1a**). These two dyes were chosen because the emission of perylene overlaps significantly with the absorption of F-PDI (**Figure 4.1b**). The experimental setup is shown in **Figure 4.1c**. Using a blue LED (408 nm) as the excitation light source, the perylene is dominately excited and its emission of the will be mostly absorbed by the F-PDI chromophore when the Janus droplets are in their natural gravity aligned orientation. When the droplets agglutinate, the fiber optic at the bottom of the sample will detect both emissions from the H (perylene) and F (F-PDI) phase chromophore. An expected ratio of the two emissions (E_H/E_F) will be correlated with the level of agglutination as the detection of the analyte concentration.

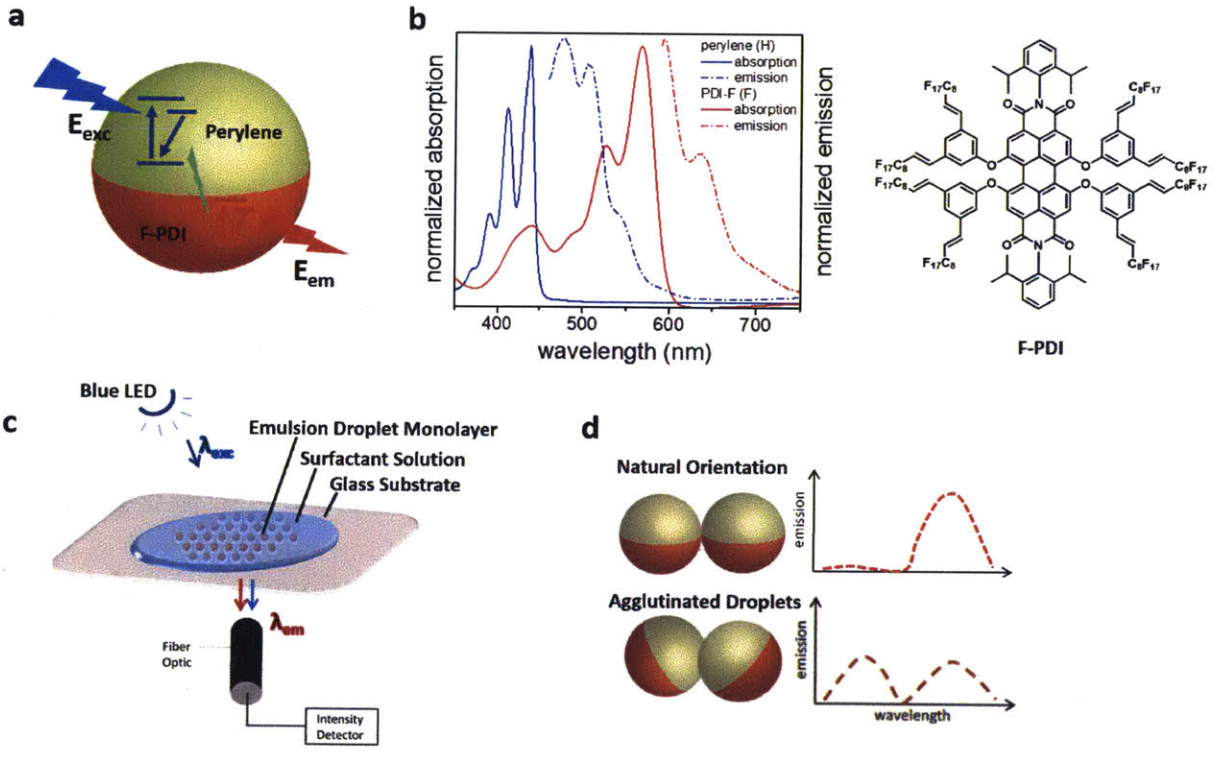

Figure 4.1. a) Scheme showing the inner filter effect with perylene in hydrocarbon phase and F-PDI in the fluorocarbon phase. b) The absorption and emission spectra of perylene and F-PDI. c) Experimental setup of the detection scheme. d) Expected emission ratio before and after droplets were agglutinated.

The agglutination assay using Sso7d and streptavidin was tested with the IFE scheme. The results is shown in **Figure 4.2**. The emission ratio readout correlate linearly with the concentration of streptavidin until the agglutination assay reaches the saturation point.

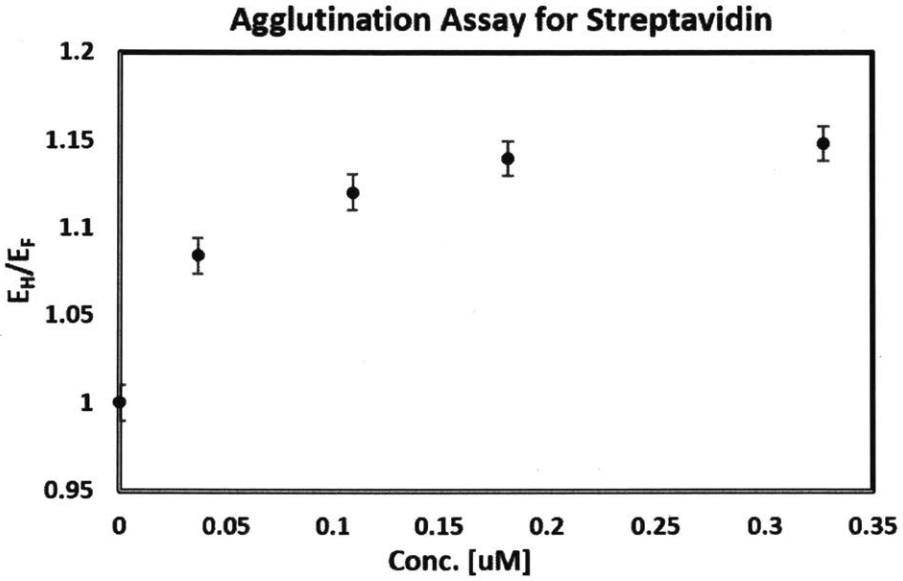

Figure 4.2. Optical readout with inner filter effect in correlation with Streptavidin concentration. The ratio E_H/E_F refers to the emitted light intensity coming from the respective hydrocarbon and fluorocarbon phases.

The agglutination assay was then expanded for the sensing of Zika NS1 protein. Another type of Sso7d (ZNS1) against Zika NS1 was synthesized and linked with a cysteine residual at the N-terminus. Because the binding strength between Zika NS1 and Sso7d (ZNS1) are not as strong as the Streptavidin and Sso7d (SA) model system, a higher concentration of Sso7d was needed in order to induce agglutination by the target. The results of NS1 detection using droplet agglutination assay was shown in **Figure 4.3**. The detection limit is 0.1 μM for a 3% emission ratio change.

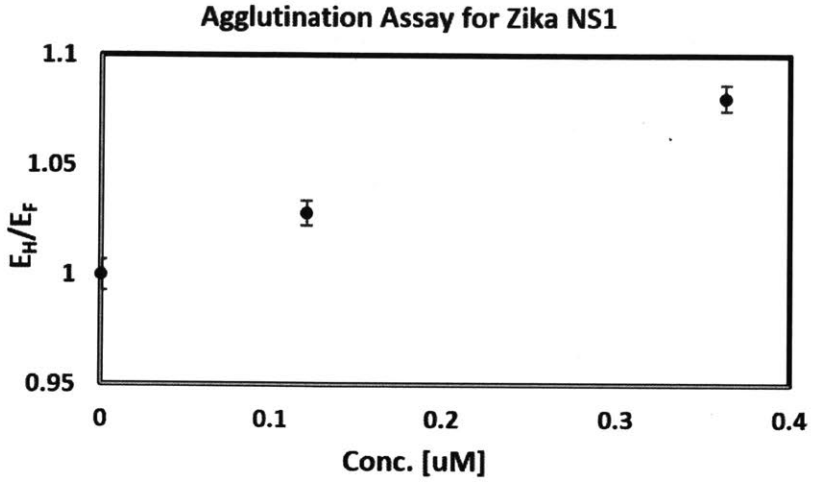

Figure 4.3. Optical readout with inner filter effect in correlation with Zika NS1 concentration.

4.3 Conclusion

In conclusion, we have reported an agglutination assay for the sensing of Zika NS1 protein at a limit of detection of 0.1 μM. A maleimide functionalized P1-MA polymer was used as the surface active agent to covalently link the hyperthermophilic Sso7d protein to the surface of the droplets. Multivalent protein analyte Zika NS1 binds multiple Sso7d on the droplet surface and agglutinates the droplets. The agglutination was detected using inner filter effect by incorporating two dyes in the hydrocarbon and fluorocarbon phase, and record the ratio of the two dye's emission intensity. This new class of emulsion agglutination assay is attractive as it has extremely low power requirements without complicated labelling and nucleic acid handling. Thus the assay can be used in extreme weather and in low resource conditions without requiring access to expensive equipment and trained personal to identify Zika virus infections.

4.4 Experimental Details

General Procedure

All chemical reagents and solvents were purchased from Sigma-Aldrich, ThermoFisher or TCI without purification unless noted otherwise. Recombinant Zika Virus NS1 protein was purchased from Abcam. Poly(styrene)-block-poly(acrylic acid) (P1) was purchased from Sigma-Aldrich. Bright field images were taken with an AmScope Inverted Microscope equipped with a digital camera.

Continuous phase surfactants were prepared as stock solution in PBS (pH = 7.6), including 0.1 wt% Zonyl FS-300 (0.1% Zonyl) as the fluorocarbon surfactant and 0.1 wt% Tween 20 (0.1% Tween) as the hydrocarbon surfactant.

The 1:1 v:v mixture of Zonyl and Tween surfactant solution was used as the surfactant washing solution (hereafter referred to as 1:1 ZT solution).

Synthesis of P1-MA

To synthesize the maleimide functionalized surfactant polymer P1-MA, a mixture of polymer P1 (50 mg, 0.00167 mmol), N-(3-Dimethylaminopropyl)-N'-ethylcarbodiimide hydrochloride (10 mg, 0.052 mmol) and 1-hydroxybenzotriazole hydrate (7 mg, 0.052 mmol) was stirred in 15 mL DMF at 0 °C for 30 min, followed by the addition of N-(2-Aminoethyl) maleimide hydrochloride (46 mg, 0.26 mmol). The reaction was stirred at room temperature overnight and the reaction mixture was precipitated into 150 mL water to get the product P1-MA.

Emulsion assay preparation

Complex emulsions, composed of equal volumes of diethylbenzene and HFE7500 in aqueous continuous phase were fabricated using bulk emulsification, which generates polydisperse droplets (20-100 μm in diameter). In this process, the hydrocarbon phase (DEB) and fluorocarbon phase (HFE 7500) were mixed and heated above the upper critical temperature (around 40 °C) to generate a single droplet phase. This single droplet phase was then dispersed into the aqueous phase containing the continuous phase surfactants to generate single phase emulsions and upon cooling to room temperature, the DEB and HFE 7500 phases separated to generate complex emulsions. The composition of all droplets was identical because every droplet originated from the same single phase.

A generic assay contains 0.5 mL of continuous phase and 20 μL droplet phase.

Sso7d functionalized emulsion assay preparation

A stock solution of Sso7d-Streptavidin (Sso7d-SA, Mw 9.26 kDa) was prepared in PBS buffer at 18 mg/mL with 10 mM tris(1-carboxyethyl)phosphine hydrochloride (TCEP). A stock solution of Sso7d-ZikaNS1 (Sso7d-ZNS1, Mw 9 kDa) was prepared in PBS buffer at 7 mg/mL with 10 mM TCEP.

Both stock solution was diluted 1000 times in 1:1 ZT solution when used as assay solution in the emulsion droplet assay.

DEB containing P1-MA at 1 mg/mL was used as the hydrocarbon phase in the emulsion assay. The continuous phase (100 μL of H and F mixture) was emulsified in 1mL 0.1% Zonyl solution. 20 μL of the droplet part of the emulsion was transferred into a vial containing 0.5 mL

Sso7d assay solution using a micropipette. The assay was stirred on a rocker (Rocker II from Boekel Scientific) for 2 h to allow the completion of the maleimide-thiol reaction.

Agglutination assay preparation with Streptavidin and Zika NS1

Lyophilized streptavidin was dissolved in PBS at 0.1 mg/mL as the analyte solution. ZS1 protein was dissolved in PBS at 270 μg/mL as the analyte solution.

The analyte solution was added to the Sso7d functionalized emulsion assay and reacted overnight before taking the optical measurement.

Experimental setup for the Inner Filter Effect

A LED light (excitation wavelength 408 nm) was used as the light source. An optical fiber was used to measure the emission from the dyes in a dark room.

4.5 References:

(1) Lanciotti, R. S.; Kosoy, O. L.; Laven, J. J.; Velez, J. O.; Lambert, A. J.; Johnson, A. J.; Stanfield, S. M.; Duffy, M. R. Genetic and Serologic Properties of Zika Virus Associated with an Epidemic, Yap State, Micronesia, 2007. *Emerg. Infect. Dis.* **2008**, *14* (8), 1232–1239.

(2) Balmaseda, A.; Stettler, K.; Medialdea-Carrera, R.; Collado, D.; Jin, X.; Zambrana, J. V.; Jaconi, S.; Cameroni, E.; Saborio, S.; Rovida, F.; Percivalle, E.; Ijaz, S.; Dicks, S.; Ushiro-Lumb, I.; Barzon, L.; Siqueira, P.; Brown, D. W. G.; Baldanti, F.; Tedder, R.; Zambon, M.; de Filippis, A. M. B.; Harris, E.; Corti, D. Antibody-Based Assay Discriminates Zika Virus Infection from Other Flaviviruses. *Proc. Natl. Acad. Sci. U. S. A.* **2017**, *114* (31), 8384–8389.

(3) Pardee, K.; Green, A. A.; Takahashi, M. K.; Braff, D.; Lambert, G.; Lee, J. W.; Ferrante, T.; Ma, D.; Donghia, N.; Fan, M.; Daringer, N. M.; Bosch, I.; Dudley, D. M.; O'Connor, D. H.; Gehrke, L.; Collins, J. J. Rapid, Low-Cost Detection of Zika Virus Using Programmable Biomolecular Components. *Cell.* **2016**, *165* (5), 1255–1266.

(4) Zarzar, L. D.; Sresht, V.; Sletten, E. M.; Kalow, J. a.; Blankschtein, D.; Swager, T. M. Dynamically Reconfigurable Complex Emulsions via Tunable Interfacial Tensions. *Nature* **2015**, *518* (7540), 520–524.

(5) Zhang, Q.; Scigliano, A.; Biver, T.; Pucci, A.; Swager, T. M. Interfacial Bioconjugation on Emulsion Droplet for Biosensors. *Bioorg. Med. Chem.* **2018**.

(6) Zhang, Q.; Savagatrup, S.; Kaplonek, P.; Seeberger, P. H.; Swager, T. M. Janus Emulsions for the Detection of Bacteria. *ACS Cent. Sci.* **2017**, *3* (4), 309–313.

(7) Nagelberg, S.; Zarzar, L. D.; Nicolas, N.; Subramanian, K.; Kalow, J. A.; Sresht, V.; Blankschtein, D.; Barbastathis, G.; Kreysing, M.; Swager, T. M.; Kolle, M. Reconfigurable and Responsive Droplet-Based Compound Micro-Lenses. *Nat. Commun.* **2017**, *8*, 14673.

(8) Brown, W. C.; Akey, D. L.; Konwerski, J. R.; Tarrasch, J. T.; Skiniotis, G.; Kuhn, R. J.; Smith, J. L. Extended Surface for Membrane Association in Zika Virus NS1 Structure. *Nat. Struct. Mol. Biol.* **2016**, *23* (9), 865–867.

(9) Miller, E. A.; Baniya, S.; Osorio, D.; Al Maalouf, Y. J.; Sikes, H. D. Paper-Based Diagnostics in the Antigen-Depletion Regime: High-Density Immobilization of rcSso7d-Cellulose-Binding Domain Fusion Proteins for Efficient Target Capture. *Biosens. Bioelectron.* **2018**, *102*, 456–463.

(10) Zarzar, L. D.; Kalow, J. A.; He, X.; Walish, J. J.; Swager, T. M. Optical Visualization and Quantification of Enzyme Activity Using Dynamic Droplet Lenses. *Proc. Natl. Acad. Sci.* **2017**, *114* (15), 201618807.

Appendix 1

NMR Spectra for Chapter 2

^{1}H NMR of ManC14 (400 MHz, $CDCl_3$)

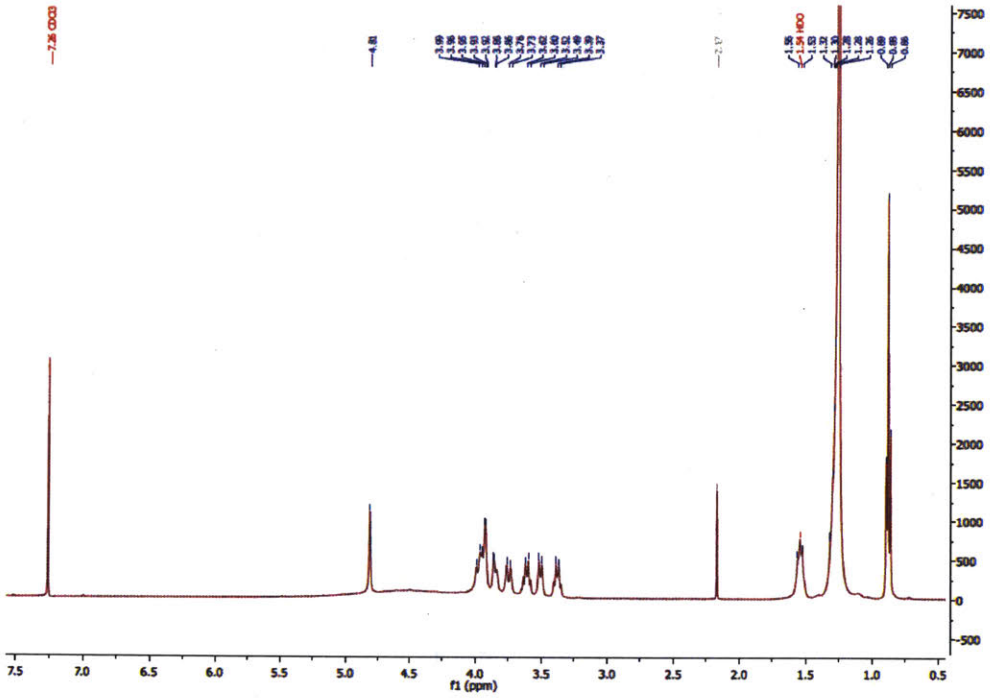

^{13}C NMR of ManC14 (400 MHz, $CDCl_3$)

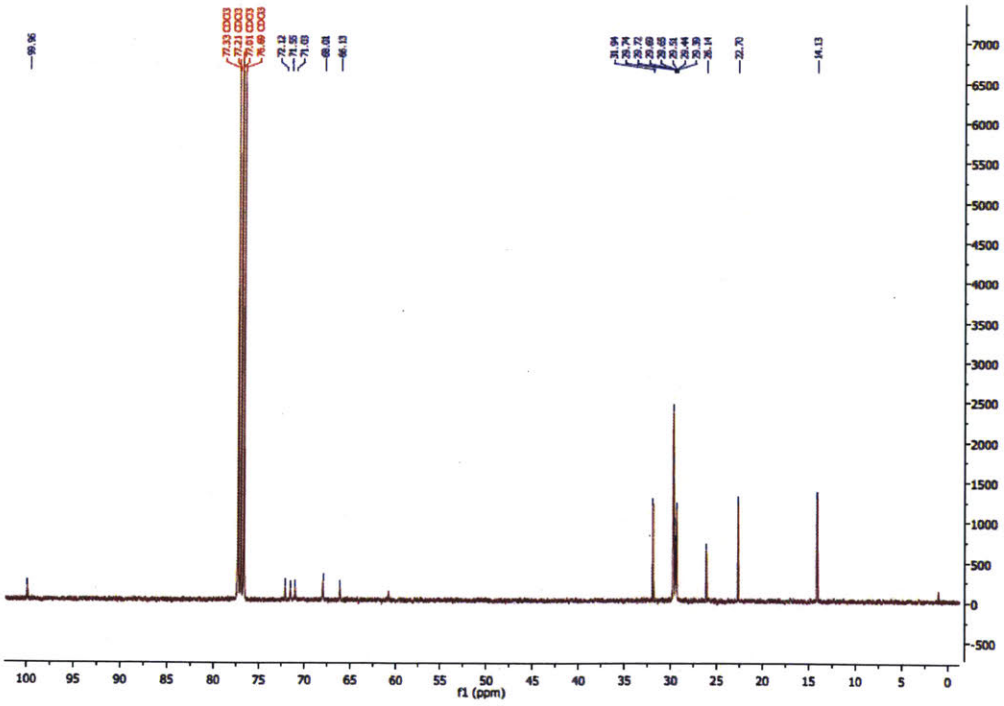

Appendix 2

NMR Spectra for Chapter 3

^{1}H NMR of GA12OH (400 MHz, $CDCl_3$)

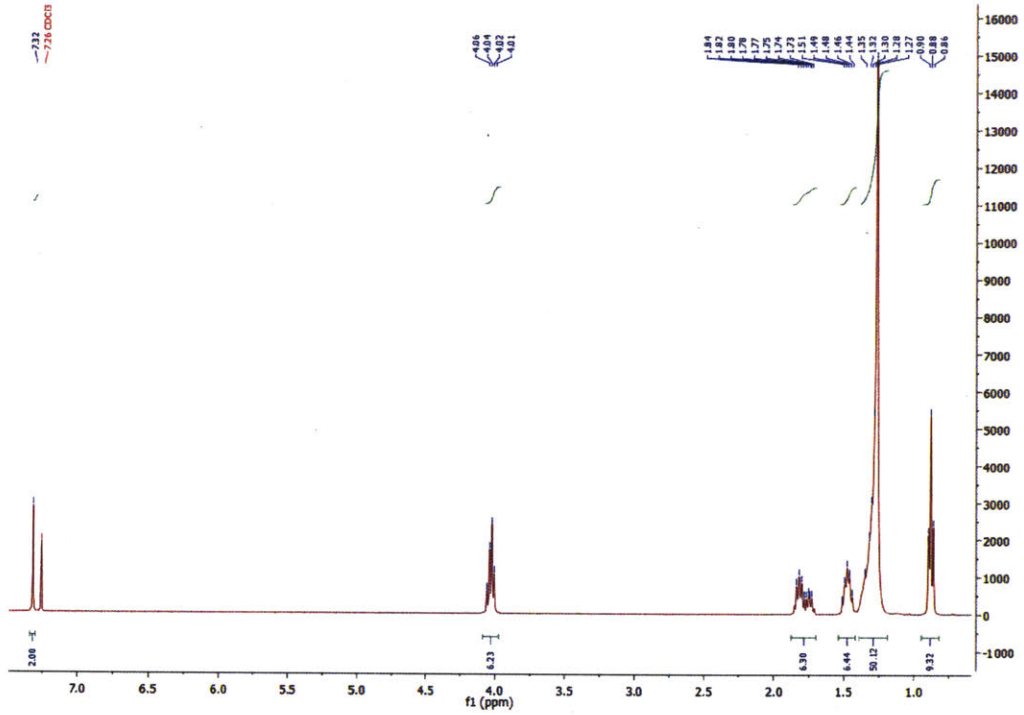

^{1}H NMR of GA12OH (400 MHz, $CDCl_3$)

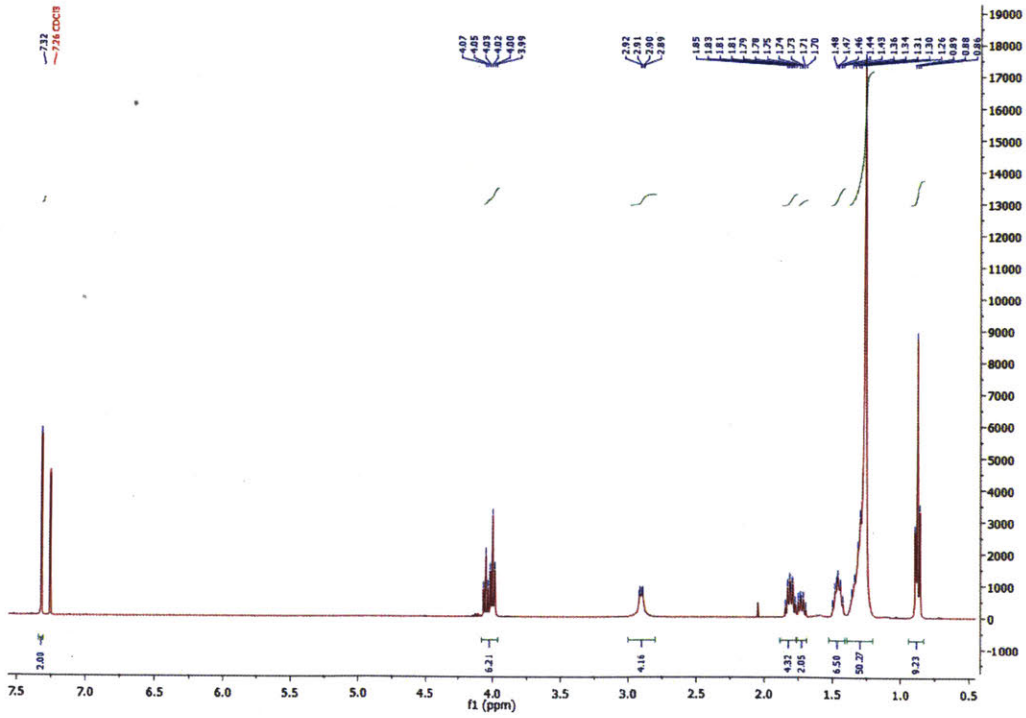

^{1}H NMR of GA16-MA (400 MHz, $CDCl_3$)

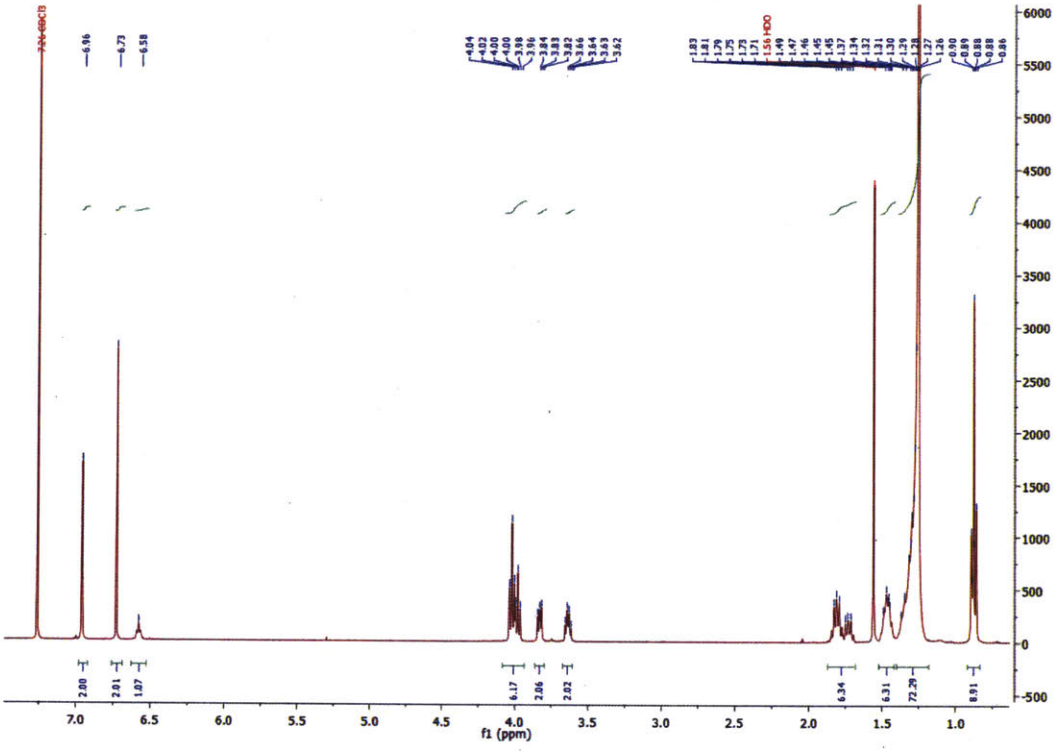

^{13}C NMR of GA16-MA (400 MHz, $CDCl_3$)

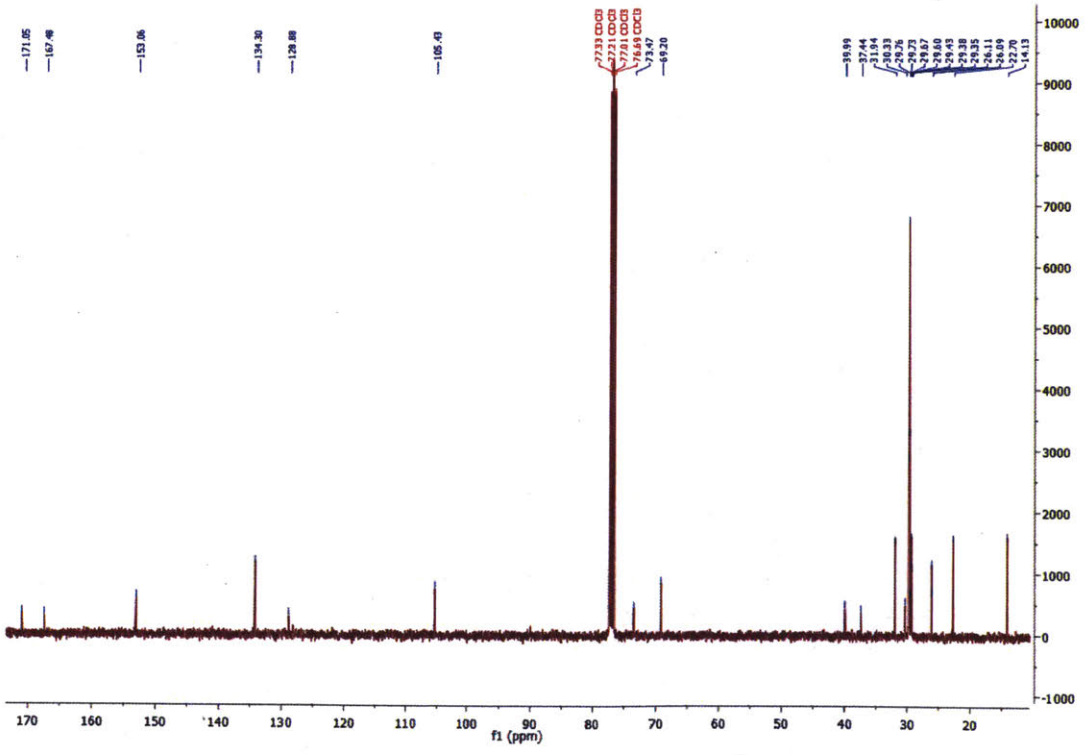

Appendix 3

IR Spectra for Chapter 3

ATR-IR Spectrum of GA16-MA (Ge)

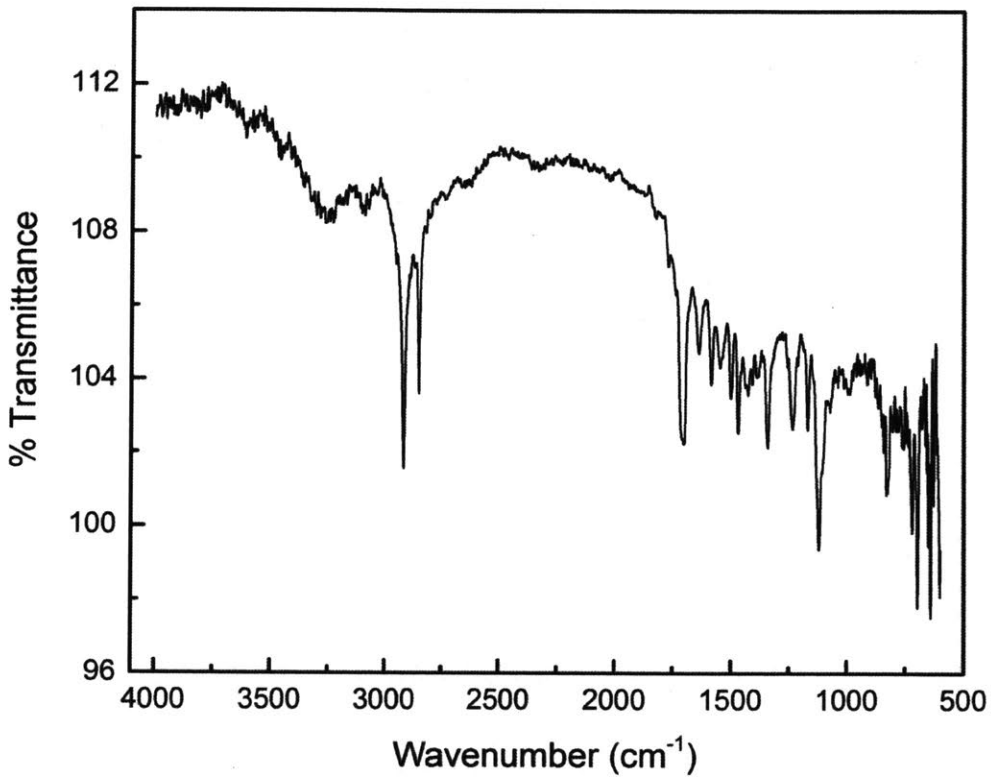

Acknowledgement

First of all, I would like to show my sincere appreciation for my academic father Tim Swager. Thank you for your patient mentorship and guidance on my research projects throughout the past four years as well as the freedom to explore different topics in several scientific areas. Thanks for your generous support and encouragement of my performances in both academic and other professional settings. I have learnt so much from you on how to be a good scientist and a good mentor. This knowledge will be invaluable to me for my future career and life.

I also want to thank my committee members, Professor Christopher Cummins and Professor Yogesh Surrendranath, for their comments and suggestions during my yearly committee meetings and the final defense. I thank Professor Hadley Sikes for her inputs on the selection of multivalent protein analytes.

The projects summarized in this thesis would not have been completed without the help of my wonderful collaborators. I have received tremendous amount of help from Dr. Suchol Savagatrup, whose solid engineering background has inspired me in many ways. I thank him for his generous help on the software and graphic designs, as well as his careful proof-reading and mentorship on writing. I also want to thank Dr. Lukas Zeininger, who has contributed several elegant optical schemes for the quantification of droplet morphology. I am enormously thankful to his help on emission measurements and sharing the stress within a tight schedule at the end of my PhD. I thank Ms. Paulina Kaplonek, Ms. Anita Scigliano, Ms. Ki-Joo Sung, and Mr. Eric Miller for their helpful feedbacks and discussions. My infinite thanks to Professor Lauren Zarzar, who taught me everything about droplets and is so generous on sharing her knowledge. I am proud to continue her legacy in the Swager team.

During my time in the Swager group, I worked closely with a group of amazing people in the colloid subgroup. I thank Ms. Cassandra Zentner, Dr. Che-Jen Lin, Mr. Yuan He, Mr. Kent Harvey, and Mr. Kosuke Yoshinaga for their contribution to the development of the colloidal platform. It was a great pleasure to work with all of you.

I am extremely grateful to Dr. Yanchuan Zhao, Dr. Rong Zhu, Dr. Sheng Chun Sha, and Dr. Byungjin Koo for being great mentors in synthetic organic chemistry and wonderful bay mates.

I want to thank my lovely officemates Dr. Bora Yoon and Mr. Wen Jie Ong, who have been great companies and resources to share joy and tears in both life and work.

I also want to thank the whole Swager group people, who have been great colleagues and friends. This is an awesome group and I am so proud to be part of the Swager family.

最后感谢我的父母。古人说，“父母在，不远游，游必有方。”感谢你们这些年来的无限支持与理解，让我虽人在异国他乡，依然能够时刻感受到家的温暖。无父何怙，无母何恃，生而有幸，当为汝说。